This is a repository copy of *A low-cost bench-top research device for turbidity measurement by radially distributed illumination intensity sensing at multiple wavelengths*.

White Rose Research Online URL for this paper:
http://eprints.whiterose.ac.uk/141481/

Version: Published Version

Hardware Article

A low-cost bench-top research device for turbidity measurement by radially distributed illumination intensity sensing at multiple wavelengths

Ben G.B. Kitchener [a],[*], Simon D. Dixon [a], Kieren O. Howarth [a], Anthony J. Parsons [b], John Wainwright [c], Mark D. Bateman [b], James R. Cooper [d], Graham K. Hargrave [e], Edward J. Long [e], Caspar J.M. Hewett [f]

[a] Department of Physics & Astronomy, University of Sheffield, United Kingdom
[b] Department of Geography, University of Sheffield, United Kingdom
[c] Department of Geography, Durham University, United Kingdom
[d] School of Environmental Sciences, University of Liverpool, United Kingdom
[e] School of Mechanical, Electrical and Manufacturing Engineering, Loughborough University, United Kingdom
[f] School of Engineering, Newcastle University, United Kingdom

ARTICLE INFO

ABSTRACT

Presented here is a new bench-top research device for the measurement of the optical turbidity of natural sediment-laden water samples. This prototype device employs 18 unique angular measurement positions and a variety of user-selectable LED light sources. The motivation for this project was the need to generate more parameter-rich data sets pertaining to the light-scattering properties of natural sediment suspensions, and to address the issues raised by Kitchener et al. (2017) concerning the inconsistent calibration methodologies currently employed to quantify suspended sediment concentration (SSC) by optical turbidity measurement. The mechanical design comprises re-purposed waste plastic materials and 3D-printed parts. The active light-source control and monitoring hardware and firmware executes on the open-source Arduino embedded microcontroller platform. The modular light sensors plug into any of the angular measurement positions, providing a 0–5 V nominal output signal, which is readable by the user's choice of data-acquisition system. The device will facilitate the highly detailed characterization of suspended sediment samples, providing 18 voltage output channels for analysis by the user. The precise calibration of the light sensors is by the use of neutral density (ND) filters in conjunction with light-source electrical current measurements, providing light-source intensity values as required. The empirical data provided by existing turbidity meters are acquired using incommensurate methodologies, and therefore they are not cross-comparable. A new methodology, described here, facilitates the cross-comparability of turbidity measurements.

© 2019 The Authors. Published by Elsevier Ltd. This is an open access article under the CC BY-NC-ND license (http://creativecommons.org/licenses/by-nc-nd/4.0/).

* Corresponding author.
  E-mail address: b.kitchener@sheffield.ac.uk (B.G.B. Kitchener).

Specifications table

Hardware name	• TARDIIS (Turbidity Assessment by Radially Distributed Illumination Intensity Sensing).
Subject area	• Environmental, Planetary and Agricultural Sciences
	• Educational Tools and Open Source Alternatives to Existing Infrastructure
Hardware type	• Measuring physical properties and in-lab sensors
Open Source License	CERN OHL, MIT
Cost of Hardware	450 GBP (ex. VAT)
Source File Repository	https://data.mendeley.com/datasets/sn3nh36k5k/1

1. Hardware in context

Commercial instruments available for the purpose of optical turbidity measurement vary widely in design, operating principle, and cost. Turbidity instruments are now ubiquitous in the water supply sector, and operate widely throughout the physical and engineering sciences (oceanography, fluvial and glacial sciences, civil engineering, chemical engineering etc.). These instruments are designed to operate either *in situ* (in a river, ocean, harbor etc.), or in a laboratory setting (*in-situ* in a flume, of off-line on a bench-top). They tend to be expensive, and they are inconsistent with regard to the measurement methodology (e.g. instrument geometry, wavelength of light source). Hence it is possible to obtain completely different and non-comparable measurements of the same water sample measured by two or more different instruments. The "turbidity units" reported by these devices are inconsistent and do not conform to the SI system of measurement, for example FNU (Formazin Nephelometric Units), NTU (Nephelometric Turbidity Units), FAU (Formazin Attenuation Units) [1].

Open-source and other public-domain instruments for turbidity measurement are available [2–6], but these devices only provide one or two measurement angles, and are limited to a single light source. In order to fully explore the limitations and capabilities of turbidity measurement it is necessary to investigate the physics of light scattering and absorption by suspended sediment, at a comprehensive range of scattering angles and wavelengths of light [1].

Designed for one specific application, these existent public-domain turbidity meters are not versatile research instruments. The list of devices presented in Table 1 is not exhaustive, but it is representative of the open-source state of the art.

Commercial instruments exist that not only measure turbidity, but also provide an estimate of the particle size distribution (PSD) of a suspension in water. In the case of suspended sediment, the determination of the PSD is by small-angle forward scattering measurements by LASER diffraction. These measurements require expensive (1000–20,000 GBP) LASER diffraction devices, which can work *in situ* or on a bench top in a laboratory.

There is a need for a research device capable of measuring the optical properties of a sediment-laden water sample and presenting the data in an unbiased format, using physically acceptable SI units (notionally mW/sr). Kitchener et al. [1] have shown that the pre-existing units of turbidity measurement (FNU, NTU, FAU etc.) are not physically valid since they are based on the mass-concentrations of arbitrary polymer suspensions, and not on the intrinsic optical properties of the particles in suspension. It was suggested [1] that research devices capable of producing multi-parameter, multi-wavelength measurements of the bulk optical properties of suspended sediment be developed, which will begin to address the issues inherent in the reporting of turbidity data and its relationship to suspended sediment concentration (SSC). TARDIIS is a first attempt at producing such an instrument. Designed for use with off-line water samples, TARDIIS operates on a laboratory bench-top. It will allow the user to observe the sediment-settling process from multiple scattering angles simultaneously, using any wavelength LED available in a 5 mm package. The user is free to interpret the measurement data in their own way, and to gain their own insights into parameters such as the PSD. The user is also encouraged to customize and refine the design to accommodate their own particular measurement requirements, and to challenge the *status quo* in terms of turbidity measurement methodology.

Table 1
Public domain turbidity instrument designs.

Authors	Instrument Geometry	Light Source	Intended Measurement Application
Lawler and Brown [2]	Direct beam	LED, Green	Suspended sediment concentration in rivers, lakes and estuaries, *in situ*.
Lambrou et al. [3]	90° nephelometric	LASER diode, Red (670 nm)	Household drinking water quality, continuous *in situ* monitoring.
Bilro et al. [4]	90° nephelometric, direct beam	LED, Red (660 nm)	Suspended sediment concentration, laboratory samples.
Kelley et al. [5]	90° nephelometric	LED, Infrared (860 nm)	Drinking water quality assessment in low-resource communities, manual samples.
Orwin and Smart [6]	180° back-scatter	LED, Infrared (880 nm)	Suspended sediment concentration in proglacial streams, *in situ*.

With a knowledge of the LED light source characteristics and a direct measurement of the LED current, TARDIIS makes it possible to report the measured light intensity in terms of appropriate SI units (mW/sr). This approach to the reporting of turbidity measurements will facilitate a more meaningful way to cross-compare measurements made on different samples by other similar devices.

2. Hardware description – TARDIIS

TARDIIS (Turbidity Assessment by Radially Distributed Illumination Intensity Sensing) is a prototype bench-top research device specifically for the examination of the light scattered by suspended sediment at multiple angles during the process of settling in a column of water, over a variable time. It is not, however, restricted to this single use-case.

TARDIIS offers:

- Turbidity measurement at 18 distinct scattering angles (with 1 LED light-source location and 35 potential sensor locations).
- Measurement of absorption and scattering in any water sample.
- User selectable light wavelengths.
- ND filter calibration.
- Data reporting in SI units (mW/sr), rather than using incommensurate turbidity units (NTU etc.). [1]
- Generation of a detailed "optical sedigraph" at multiple wavelengths.

3. Design files

The link to the top-level folder for this project on Mendelay Data is DOI: https://data.mendeley.com/datasets/sn3n-h36k5k/1

3.1. Design files summary – TARDIIS electronics schematics & drawings

Design file name	File type	Description	Open source license	Location of the file
Amplifier. dch	'DipTRACE Schematic.	Photodiode Amplifier DipTRACE schematic.	CERN OHL	https://data.mendeley.com/datasets/sn3nh36k5k/1#file-033bcadb-eb6d-4faf-b010-1004630e09bc
Amplifier. dip	DipTRACE PCB layout.	Photodiode Amplifier DipTRACE PCB layout.	CERN OHL	https://data.mendeley.com/datasets/sn3nh36k5k/1#file-18b6a683-3f32-4286-8d2b-abb31f5b8298
LED Driver Arduino Shield.dch	'DipTRACE Schematic.	LED Control & Monitoring Shield DipTRACE schematic.	CERN OHL	https://data.mendeley.com/datasets/sn3nh36k5k/1#file-91fba345-8b47-4b20-a740-fdab1ae48320
LED Driver Arduino Shield.dip	DipTRACE PCB layout.	LED Control & Monitoring Shield PCB DipTRACE layout.	CERN OHL	https://data.mendeley.com/datasets/sn3nh36k5k/1#file-3a49c4f4-b2a0-486c-a0b5-84bbaca56b5a
Turbidity.eli	DipTRACE schematic symbol library.	DipTRACE schematic symbol library for Photodiode Amplifier and the LED Control & Monitoring Shield.	CERN OHL	https://data.mendeley.com/datasets/sn3nh36k5k/1#file-2f97a2fb-05c4-4f87-b23a-94600e8658b8
Turbiity.lib	DipTRACE PCB symbol library.	DipTRACE PCB symbol library for Photodiode Amplifier and the LED Control & Monitoring Shield.	CERN OHL	https://data.mendeley.com/datasets/sn3nh36k5k/1#file-d90d4767-19c4-4af1-a15d-772e2f426d2e
1053131203. stp	STEP File.	Molex connector STEP file.	CERN OHL	https://data.mendeley.com/datasets/sn3nh36k5k/1#file-f1e182eb-fe4b-47cb-ac60-b3659dc099a6

The DipTRACE design files are provided so that the user can easily modify the existing circuits using the DipTRACE CAD package.

3.2. Design files summary – TARDIIS electronics Gerbers

Design file name	File type	Description	Open source license	Location of the file
Active_LED_Control_ Application	Gerber	Folder containing LED Control & Monitoring Shield Gerbers.	CERN OHL	https://data.mendeley.com/datasets/ sn3nh36k5k/1#folder-c7770cfd-b5d9-415a- baf0-ec76d2acdc0a
Amplifier_Gerbers	Gerber	Folder containing Photodiode Amplifier Gerbers.	CERN OHL	https://data.mendeley.com/datasets/ sn3nh36k5k/1#folder-6bdbf85c-8fe3-4efe- 9df2-2b155f2dc179

4 The Gerber files can be sent directly to a manufacturer for PCB production.

3.3. Design files summary – TARDIIS LED control & monitoring shield firmware

Design file name	File type	Description	Open source license	Location of the file
Active_LED_Control_ Application.ino	Arduino source code	Active_LED_Control_Application Arduino Firmware	MIT	https://data.mendeley.com/datasets/ sn3nh36k5k/1#file-ea7f2a61-7a4b- 4fa9-83e8-a19ca04baffb

3.3.1. Design files summary – TARDIIS mechanical – OpenSCAD files

Design file name	File type	Description	Open source license	Location of the file
Amplifier_housing. scad	OpenSCAD	OpenSCAD source file for photodiode amplifier/LED housing.	CERN OHL	https://data.mendeley.com/datasets/ sn3nh36k5k/1#file-ab9e9b4f-7d91-46c6- 8f95-640a6c1317e1
Photodiode_Calibrator. scad	OpenSCAD	OpenSCAD source file for photodiode calibrator.	CERN OHL	https://data.mendeley.com/datasets/ sn3nh36k5k/1#file-4e142e20-d620- 435c-acc6-7d40a5ab6076
Amplifier_housing	STL	Photodiode amplifier housing STL, created in OpenSCAD.	CERN OHL	https://data.mendeley.com/datasets/ sn3nh36k5k/1#file-77fc7e42-5de2-4268- 874f-abc9615594e2
Photodiode_Calibrator	STL	Photodiode calibrator STL, created in OpenSCAD.	CERN OHL	https://data.mendeley.com/datasets/ sn3nh36k5k/1#file-a8ba5a56-95be- 4938-b2ed-853ea9c6c34a

The 3D printed parts were originally created using OpenSCAD, which can be used to open and modify the designs. The STL files were generated by OpenSCAD, and can be directly uploaded to a 3D printer for printing. These designs have also been re-drawn in SolidWorks in order to produce 2D drawings (as PDF files (3.5)) of the parts, as this function is not available in OpenSCAD.

3.4. Design files summary – TARDIIS mechanical – drawings & SolidWorks files

Design file name	File type	Description	Open source license	Location of the file
Amplifier Housing.pdf	PDF	Drawings of photodiode amplifier/LED housing.	CERN OHL	https://data.mendeley.com/datasets/sn3nh36k5k/1#file-4309487b-1d00-4825-ab4e-9fc4eec86253
Assembly.pdf	PDF	Drawings of the complete TARDIIS assembly.	CERN OHL	https://data.mendeley.com/datasets/sn3nh36k5k/1#file-720a42ab-4a33-41ee-ba96-27fc175d1a89
Photodiode_Calibrator Part 1.pdf	PDF	Drawings of the photodiode calibrator module receptacle sections.	CERN OHL	https://data.mendeley.com/datasets/sn3nh36k5k/1#file-98e5acba-36b4-416b-8e03-6ec6bd0c898d
Photodiode_Calibrator Part 2.pdf	PDF	Drawings of the photodiode calibrator module ND filter housing section.	CERN OHL	https://data.mendeley.com/datasets/sn3nh36k5k/1#file-68102f66-ca28-456f-83c2-c1eee9ed2d41
Base.pdf	PDF	Drawings of TARDIIS base section.	CERN OHL	https://data.mendeley.com/datasets/sn3nh36k5k/1#file-14b05145-5241-4bd4-878b-0c173ad94033
Sensor collar.pdf	PDF	Drawings of TARDIIS sensor collar section.	CERN OHL	https://data.mendeley.com/datasets/sn3nh36k5k/1#file-d4a9723a-095e-474c-a90a-125d674e4b9d
Sensor Ring.pdf	PDF	Drawings of TARDIIS sensor ring section.	CERN OHL	https://data.mendeley.com/datasets/sn3nh36k5k/1#file-4bc72e51-08ea-490b-ae22-543aebd59ef6
Amplifier Housing.sldd	SLDD	SolidWorks Drawings of photodiode amplifier/LED housing.	CERN OHL	https://data.mendeley.com/datasets/sn3nh36k5k/1#file-ac049fce-69ad-4e83-9759-ef609a57cb0a
Assembly.sldd	SLDD	SolidWorks Drawings of the complete TARDIIS assembly.	CERN OHL	https://data.mendeley.com/datasets/sn3nh36k5k/1#file-1cb6d8db-1993-4038-beff-fe1e677e2cbf
Photodiode_Calibrator Part 1. sldd	SLDD	SolidWorks Drawings of the photodiode calibrator module receptacle sections.	CERN OHL	https://data.mendeley.com/datasets/sn3nh36k5k/1#file-eabf0021-5443-4109-a0bd-f211932f4ac0
Photodiode_Calibrator Part 2. sldd	SLDD	SolidWorks Drawings of the photodiode calibrator module ND filter housing section.	CERN OHL	https://data.mendeley.com/datasets/sn3nh36k5k/1#file-08be4caa-2d8b-48db-be89-f88fc9542322
Base.sldd	SLDD	SolidWorks Drawings of TARDIIS base section.	CERN OHL	https://data.mendeley.com/datasets/sn3nh36k5k/1#file-8b46d655-79fa-4c5a-9843-d23d5c8f4414
Sensor collar.sldd	SLDD	SolidWorks Drawings of TARDIIS sensor collar section.	CERN OHL	https://data.mendeley.com/datasets/sn3nh36k5k/1#file-284e41c6-4481-4c7b-86ac-aceec1ebcc5d
Sensor Ring.sldd	SLDD	SolidWorks Drawings of TARDIIS sensor ring section.	CERN OHL	https://data.mendeley.com/datasets/sn3nh36k5k/1#file-08edcc93-3ab4-451c-8d12-0982bb06e067

The PDF design files can be handed directly to a machinist for production of the parts. Alternatively, the SolidWorks files will allow the user to make modifications to the designs using the SolidWorks CAD package.

4. Bill of materials

4.1. Bill of materials – TARDIIS mechanical (see Fig. 1 drawing designations)

Designator	Component	Number	Cost per unit – GBP	Total cost – GBP	Source of materials	Material type
#1, #3, #4 *	PVC Grey Sheet 500 × 250 × 20 mm	1	26.16	26.16	https://www.directplastics.co.uk/pvc-sheet	Polymer
#2a	(100/94) 100 mm × 3 mm × 500 mm Clear Acrylic Tube (Extruded)	1	10.83	10.83	http://clearplastictube.co.uk/index.php?route=common/home	Polymer
#2b	100 mm DIA × 3 mm thick Clear Acrylic Disc	1	2.10	2.10	http://clearplastictube.co.uk/index.php?route=common/home	Polymer
#2c	EMA Plastic Weld 57 ml	1	4.99	4.99	http://clearplastictube.co.uk/index.php?route=common/home	Organic
#5	RS Pro Stainless Steel, Hex Nut, M8	1 bag of 50 (6 needed)	8.79	8.79	https://uk.rs-online.com/web/p/hex-nuts/0189608/	Metal
#6	Stainless Steel Plain Washer, 1 mm Thickness, M8 (Form B), A4 316	1 bag of 50 (6 needed)	4.78	4.78	https://uk.rs-online.com/web/p/plain-washers/0189664/	Metal
#7	RS Pro Plain Stainless Steel Threaded Rod, M8, 1 m	Each in a pack of 5 (2 needed)	3.81	19.05	https://uk.rs-online.com/web/p/threaded-rods-studs/0280408/	Metal
#8 **	RS Pro 1.75 mm Black PLA 3D Printer Filament, 300 g	1	10.42	10.42	https://uk.rs-online.com/web/p/3d-printing-materials/8320406/	Polymer
			Subtotal:	**87.12 (ex VAT)**		

*The base, sensor collar and sensor ring could all potentially be manufactured from this material. Other similar materials could be substituted (e.g. nylon).
**This is an example of PLA filament used for 3D printing the sensor/LED housing and the photodiode calibrator. The filament chosen for this purpose must be compatible with the particular 3D printer used for making any parts.

4.2. Bill of materials – TARDIIS electronics – LED control & monitoring shield

Designator	Component	Number	Cost per unit – GBP	Total cost – GBP	Source of materials	Material type
ARD1	Arduino UNO	1	16.64	16.64	https://uk.rs-online.com/web/p/processor-microcontroller-development-kits/7154081/	Other: Electronics
U1	STMicroelectronics LM317P Linear Voltage Regulator, 1.5A, Adjustable, 1.2 → 37 V 3-Pin, TO-220FP	Each in a pack of 10 (1 needed)	0.62	6.20	https://uk.rs-online.com/web/p/linear-voltage-regulators/6869717/	Semiconductor

Bill of materials – TARDIIS electronics – LED control & monitoring shield (*continued*)

Designator	Component	Number	Cost per unit – GBP	Total cost – GBP	Source of materials	Material type
U2	MCP4261-502E/P – Non Volatile Digital Potentiometer, 5 kohm, Dual, SPI, Linear, ±20%, 2.7 V	1	0.94	0.94	http://uk.farnell.com/microchip/mcp4261-502e-p/ic-dgtl-pot-5k-2ch-14dip/dp/1840760	Semiconductor
U3	MAX1416EPE+ – Analogue to Digital Converter, Low Power, 16 bit, 500 SPS, Single, 2.7 V, 3.6 V, DIP	1	6.26	6.26	http://uk.farnell.com/maxim-integrated-products/max1416epe/adc-2-ch-sigma-delta-16bit-dip/dp/2513557	Semiconductor
U4	MAX6225ACPA+ – Voltage Reference Series – Fixed, 2.5 V reference, ±1 ppm/°C, DIP-8	1	5.16	5.16	http://uk.farnell.com/maxim-integrated-products/max6225acpa/voltage-ref-series-2-5v-dip-8/dp/2511205	Semiconductor
J1, J2	105313-1203 – Wire-To-Board Connector, Right Angle, 2.5 mm, 3 Contacts, Header, Nano-Fit Series, Through Hole	2	0.78	1.56	http://uk.farnell.com/molex/105313-1203/connector-header-3pos-1row-2-5mm/dp/2576867	Metal/Polymer
Connector housing for sensors & LEDs	105307-1203 – Connector Housing, TPA Capable, Nano-Fit Series, Receptacle, 3 Ways, 2.5 mm	30[*]	0.22	6.60	http://uk.farnell.com/molex/105307-1203/receptacle-housing-3pos-nylon/dp/2576853	Metal/Polymer
Pins for Molex connectors	105300-1200 – Contact, 6.5A/300 V, Nano-Fit Series, Socket, Crimp, 24 AWG, Gold Plated Contacts	100	0.14	14.00	http://uk.farnell.com/molex/105300-1200/contact-socket-26-24awg-crimp/dp/2576850	Metal
R1	Vishay RN65 Series Axial Metal Film Fixed Resistor 250 Ω ± 0.1% 0.5 W ± 50 ppm/°C	1	0.75	0.75	https://uk.rs-online.com/web/p/through-hole-fixed-resistors/8500696/	Metal
R2	TE Connectivity LR1 Series Axial Metal Film Fixed Resistor 100 Ω ± 1% 0.6 W ± 50 ppm/°C	Each in a pack of 10 (1 needed)	0.08	0.80	https://uk.rs-online.com/web/p/through-hole-fixed-resistors/0148269/	Metal
R3	http://uk.farnell.com/bourns/pwr220t-20-1r50f/resistor-thick-film-1-5ohm-1-to/dp/2328253	1	4.82	4.82	http://uk.farnell.com/bourns/pwr220t-20-1r50f/resistor-thick-film-1-5ohm-1-to/dp/2328253	Metal

(*continued on next page*)

Bill of materials – TARDIIS electronics – LED control & monitoring shield (*continued*)

Designator	Component	Number	Cost per unit – GBP	Total cost – GBP	Source of materials	Material type
C1, C2, C6	KEMET 100nF Multilayer Ceramic Capacitor MLCC 50 V dc ±10% X7R Dielectric Radial, Max. Temp. +125 °C	Each in a pack of 5 (3 needed)	0.19	0.57	https://uk.rs-online.com/web/p/ceramic-multilayer-capacitors/5381310/	Ceramic
C3	Murata 10μF Multilayer Ceramic Capacitor MLCC 50 V dc ±20% X7R Dielectric Radial Through Hole, Max. Temp. +125 °C	Each in a pack of 5 (1 needed)	1.65	8.25	https://uk.rs-online.com/web/p/ceramic-multilayer-capacitors/8118373/	Ceramic
C4, C5	Murata 2.2 μF Multilayer Ceramic Capacitor MLCC 50 V dc ±15% X7R Dielectric Radial Through Hole, Max. Temp. +125 °C	Each in a pack of 10 (2 needed)	0.31	3.10	https://uk.rs-online.com/web/p/ceramic-multilayer-capacitors/8410758/	Ceramic
Cable for sensors & LEDs	9533 – Multicore Screened Cable, Computer, EIA RS-232, Per Metre, 3 Core, 24 AWG, 0.2 mm^2, Chrome	Per metre (15 m needed[**])	1.06	15.90	http://uk.farnell.com/belden/9533/cable-9533-3core-per-m/dp/1218691	Metal/Polymer
Header for Arduino UNO connection	RS Pro, 2.54 mm Pitch, 36 Way, 1 Row, Straight Pin Header, Through Hole	1	0.37	0.37	https://uk.rs-online.com/web/p/pcb-headers/2518632/	Metal/Polymer
			Subtotal:	**91.92 (ex VAT)**		

[*]Number depends on requirements, for example 24 are needed for making 18 sensor modules and 6 LED modules, with 6 spare.

[**]Number depends on requirements. For example, 15 m is enough for 18 sensor modules with 50 cm cable lengths, plus 6 LED modules and some spare for making a power cable.

4.3. Bill of materials – TARDIIS electronics – photodiode amplifier

Designator	Component	Number	Cost per unit – GBP	Total cost – GBP	Source of materials	Material type
U1	MCP6491T-E/OT – Operational Amplifier, Single, 1 Amplifier, 7.5 MHz, 6 V/μs, 2.4 V to 5.5 V, SOT-23, 5 Pins	18[*]	0.84	15.12	http://uk.farnell.com/microchip/mcp6491t-e-ot/op-amp-5-5v-7-5mhz-6v-us-5sot23/dp/2306614	Semiconductor
R1[**]	RC0805JR-07100ML – SMD Chip Resistor, 100 Mohm, RC Series, 150 V, Thick Film, 0805 [2012 Metric], 125 mW	18[*] (20 min order)	0.12	2.40	http://uk.farnell.com/yageo/rc0805jr-07100ml/res-thick-film-100m-5-0-125w-0805/dp/9236511	Metal

Bill of materials – TARDIIS electronics – photodiode amplifier (*continued*)

Designator	Component	Number	Cost per unit – GBP	Total cost – GBP	Source of materials	Material type
C1***	AVX 22pF Multilayer Ceramic Capacitor MLCC 200 V dc 0805, Max. Temp. +125 °C	18* (100 min order)	0.073	7.30	https://uk.rs-online.com/web/p/ceramic-multilayer-capacitors/1356624/	Ceramic
C2***	Kemet-BHC 100nF Multilayer Ceramic Capacitor MLCC 100 V dc ±10% X7R Dielectric 0805 Solder, Max. Temp. +125 °C	18* (100 min order)	0.06	6.00	https://uk.rs-online.com/web/p/ceramic-multilayer-capacitors/1744482/	Ceramic
PD1	SFH213 – Photodiode, 10°, 1nA, 850 nm, T-1 3/4 (5 mm)	18* (20 – multiples of 5)	0.56	11.20	http://uk.farnell.com/osram-opto-semiconductors/sfh213/photodiode-850nm-10-t-1-3-4-5mm/dp/1212761	Semiconductor
			Subtotal:	**42.02 (ex VAT)**		

*Number depends on requirements. We recommend purchasing 50% more of these than are required by the design, as they are easy to break or lose.

**The resistor R1 determines the gain of the amplifier. We used the 100 M value listed here for a very high gain; however, the user is free to use lower resistances to achieve lower gains.

***These capacitors are optional. We did not use them in our application. The values here are examples.

4.4. Bill of materials – TARDIIS electronics – sundry items

Designator	Component	Number	Cost per unit – GBP	Total cost – GBP	Source of materials	Material type
3.0 ND	3.0 OD 25 mm Diameter, Reflective ND Filter Stock #43-812	1	40.38	40.38	https://www.edmundoptics.co.uk/p/30-od-25mm-diameter-reflective-nd-filter/5303/	Glass/Metal
4.0 ND	4.0 OD 25 mm Dia., NIR ND Filter Stock #36-266	1	80.75	80.75	https://www.edmundoptics.co.uk/p/40-OD-25mm-Dia-NIR-ND-Filter/37226/	Glass/Metal
			Subtotal:	**121.13 (ex VAT)**		

4.5. PCB fabrication

The PCBs used in this project were fabricated by Ragworm [7]. The price per PCB depends on its size, and the number ordered. We purchased two of the LED Control & Monitoring Shield PCBs for 31.83 GBP (one was a spare). We also purchased 50 of the Photodiode Amplifier PCBs for 39.06 GBP.

5. Build instructions – mechanical

5.1. Sample cell, sensor collar and mounting system

The sample cell (#2) consists of an extruded acrylic tube (#2a) 491 mm in length, with an internal diameter of 93 mm, and an external diameter of 100 mm. An acrylic disc (#2b) is glued (#2c) to one end of the tube to close it and form the watertight bottom of the sample cell. The sample cell then sits in the recessed base (#1) of the mounting system, surrounded
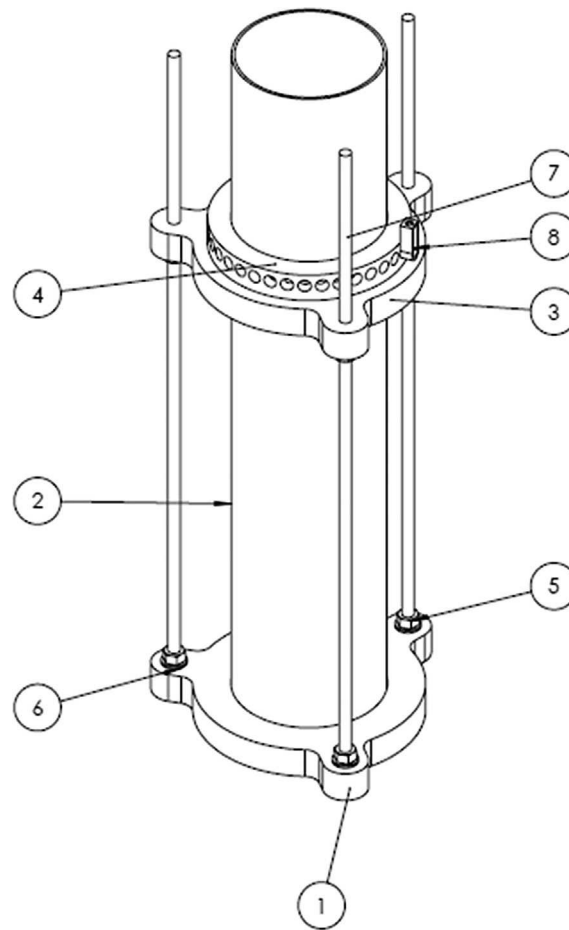
Fig. 1. TARDIIS assembly drawing. #1) Base. #2) Tube (sample cell). #3) Sensor collar. #4) Sensor ring. #5) M8 nut. #6) M8 washer. #7) Threaded rod. #8) Amplifier housing.

by the three support columns (#7). The height of the nuts (#5 – see Fig. 2 for positions) on the support columns can be adjusted to alter the height of the sensor collar (#3) containing the sensor ring (#4) above the base plate, which slots onto the support columns and encapsulates the circumference of the sample cell (Figs. 1, 2). This arrangement allows turbidity measurements to be performed at any height in the water column containing the sediment sample. The amplifier housing (#8) may contain either a photodiode amplifier PCB, or an LED.

5.2. Sample cell

The sample cell is made from an extruded acrylic tube (#2a), and has an acrylic disc glued (#2b) to one end to form the bottom of the cell. We found that the acrylic disc had a slightly larger diameter than the acrylic tube. After gluing the disc onto the tube, we had to perform some manual filing of the disc circumference to bring it flush with the tube diameter. This was necessary to allow the whole tube to fit easily through the sensor collar, thus allowing clearance for its lifting in and out of the instrument assembly without snagging on the sensor ring.

5.3. Sensor ring

The sensor ring (Fig. 3) fits over the outer diameter of the sample cell to facilitate the connection of LED light modules and sensor modules at any of the 36 receptacle positions around the circumference of the ring, at 10° intervals. The receptacle positions each consist of an 8.7 mm diameter hole in the outer surface of the ring, bored to a depth of 10 mm. This hole allows a 3D-printed sensor housing (which could contain either a photodiode amplifier or an LED) to be slotted in and held in place by an interference fit. A second concentric hole of 3 mm diameter then penetrates through the remaining thickness of the sensor ring wall and breaks through to the inner surface of the sensor ring, to form a collimated light path. This collimator hole helps to eliminate stray light when a sensor module is connected, and provides a consistent angle of maximum beam divergence for any given type of LED utilized as a light source.
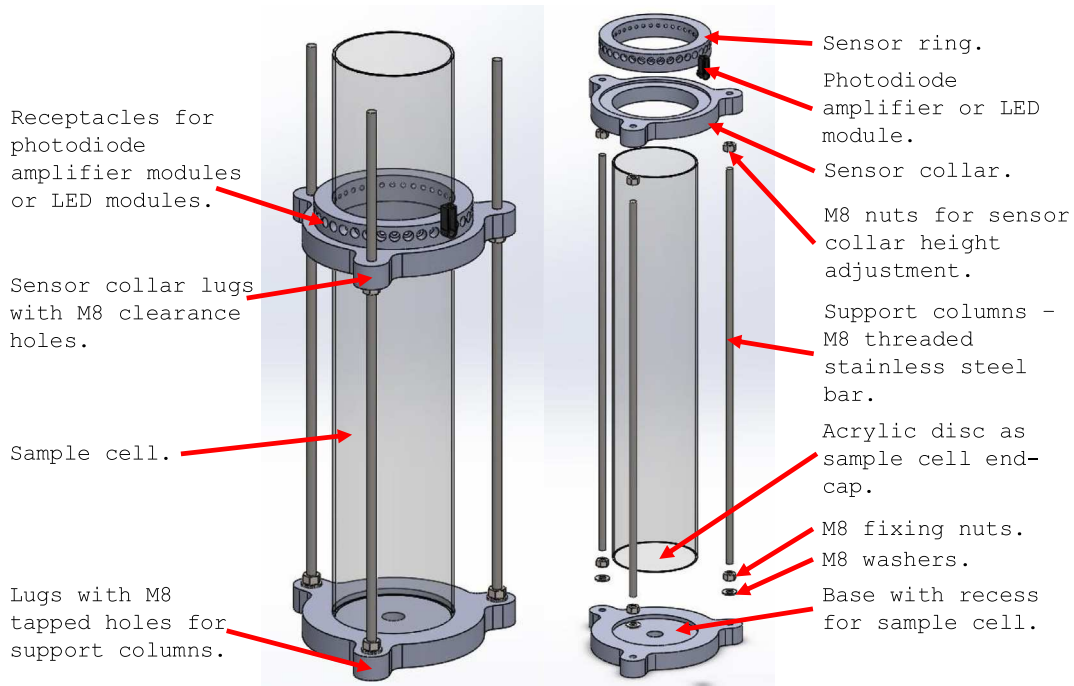
Fig. 2. TARDIIS instrument assembly (left) and exploded view (right) showing the mounting system with support columns for the sensor collar containing the sensor ring.

The sensor ring was machined from waste nylon plastic (Fig. 4), and the sensor collar into which it fits was made from waste PVC, although both parts could be made from the same stock. Alternative materials could be used to create these parts, e.g. wood or MDF, or any suitably rigid and machineable material.

5.4. Sensor collar

The sensor collar (Fig. 5) has lugs with M8 clearance holes that allow it to slot onto the support columns of the main assembly, thus allowing the sensor ring to encircle the sample cell when contained by the collar (Fig. 6).

5.5. Base

The base (Fig. 7) has lugs with M8 threaded holes that allow the support columns to be screwed in and then locked in place with M8 nuts and washers. A 5 mm deep recess allows for sample cell lateral retention at the bottom end.
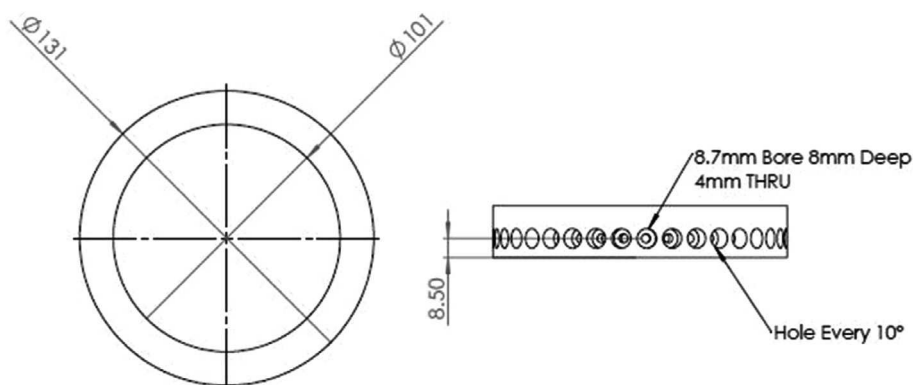
Fig. 3. Sensor ring drawings.
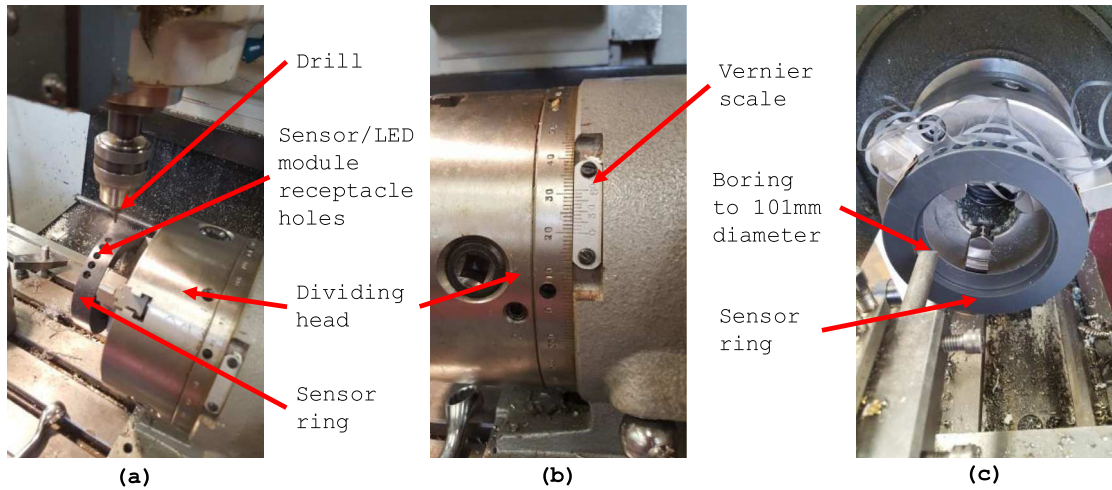
Fig. 4. a) Drilling of sensor/LED module receptacle holes in the sensor ring, shown mounted in a dividing head to produce a regular separation angle of 10°. Centre drilled through at 4 mm diameter (inner collimator hole), and then counter bored at 8.7 mm diameter to 8 mm depth (module receptacle hole). b) The Vernier scale on the dividing head showing the setting required to achieve the 10° separation angle. c) The boring of the internal diameter of the sensor ring to 101 mm so that it will fit over the 100 mm outer diameter of the sample cell.
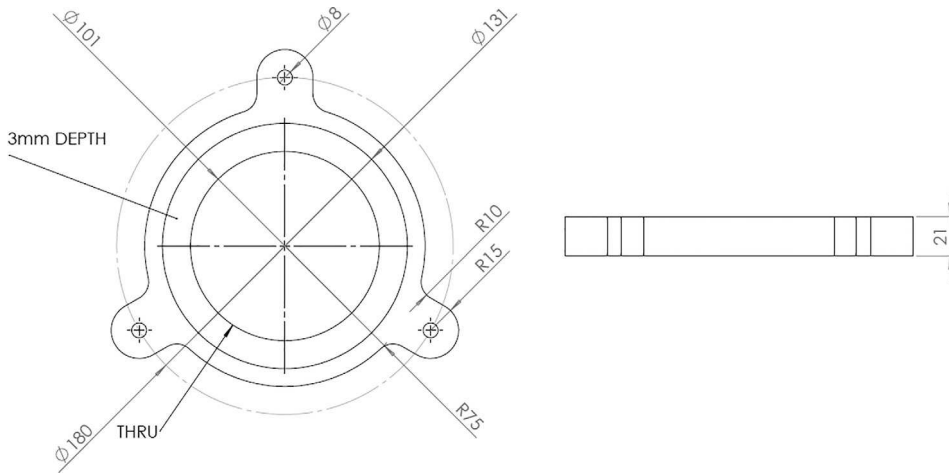
Fig. 5. Sensor collar drawings.
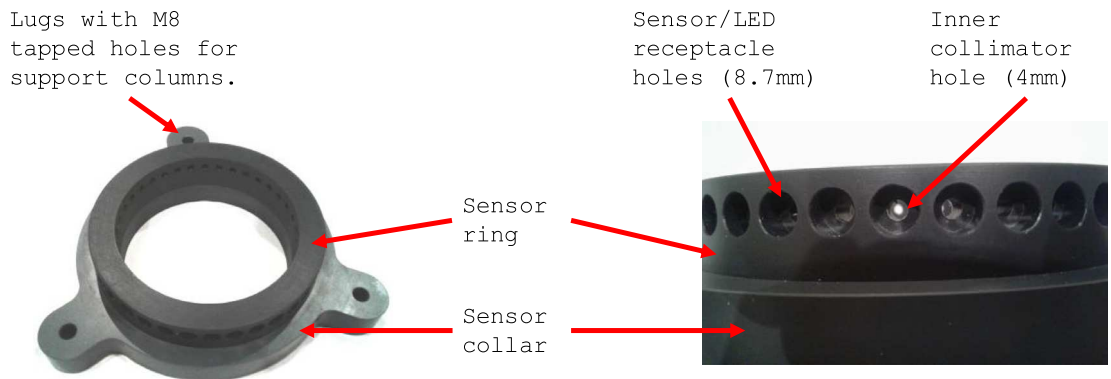
Fig. 6. The sensor ring mounted in the sensor collar. The sensor/LED module receptacle holes (8.7 mm diameter) are shown along with the concentric 4 mm diameter inner collimator holes.

5.6. Sensor and LED modules

The small form-factor of the sensor/LED housing measuring only 27.5 × 10.5 × 13.5 mm, as shown in Fig. 8.

The sensor module consists of the photodiode amplifier board and a plastic housing for it, which was designed using OpenSCAD [8] and printed on a Makerbot 3D printer from PLA plastic (Fig. 9). As the photodiode amplifier utilises an SFH213 photodiode in a standard 5 mm package, the same plastic module can be used to house an LED with the same standard 5 mm package.

5.7. Photodiode calibrator and ND filters

The principle of operation of the optical calibrator is the measurement of the attenuation of a light source by the placing of an optical neutral density filter (ND filter) between the light source (LED module) and the detector (sensor module), as in Fig. 10. It is worth noting that the filter number *ND* is synonymous with absorbance, *A* (see Kitchener et al., p.628 for an explanation of absorbance [1]).
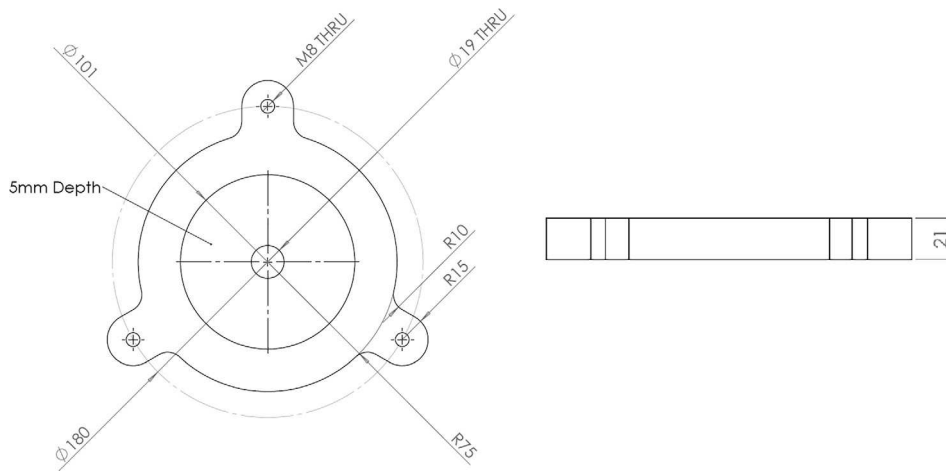
Fig. 7. Base drawings.
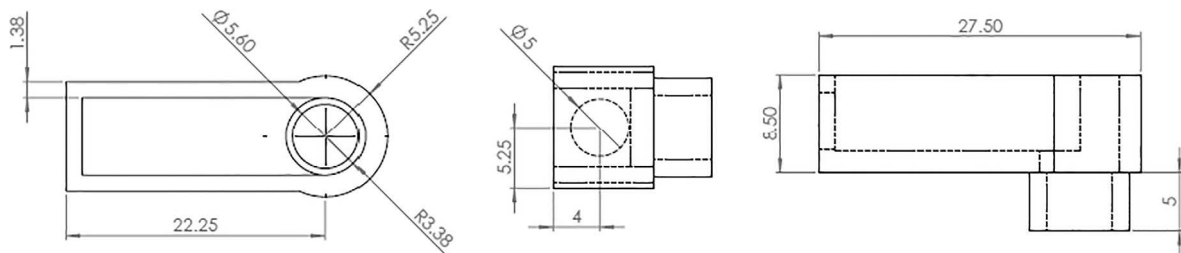
Fig. 8. Sensor or LED module housing drawings.
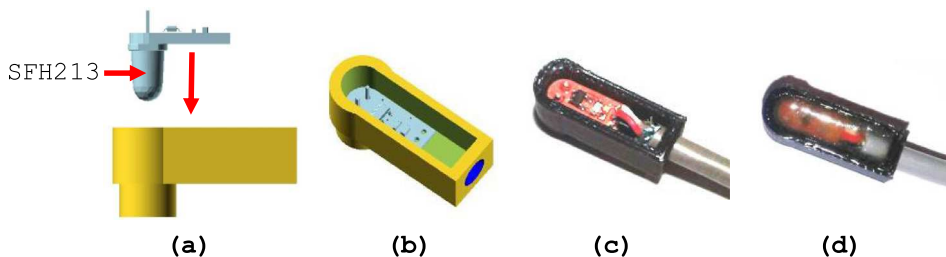
Fig. 9. a) CAD model showing the photodiode amplifier PCB insertion into the module housing. b) A CAD model of the PCB located in the housing. c) The actual photodiode amplifier located in the 3D-printed module housing with cable attached. d) The module potted with epoxy resin.

The percentage of light transmitted by an ND filter is T:

$$\frac{I}{I_0} = T(\%) = 10^{-ND} \times 100 \tag{1}$$

For example, a 3.0 ND filter will transmit 0.1% of the incident light, whereas a 0.3 ND filter will transmit 50.12% of the incident light. The transmission formula in terms of the ND filter number is:

$$ND = -\log \frac{T(\%)}{100} \tag{2}$$

The photograph in Fig. 11 demonstrates the logarithmic nature of the relationship between percent transmission and ND filter number.

5.8. Photodiode calibrator design

The photodiode calibrator consists of two different parts, designed to be printed separately on a filament type 3D printer. Part 1 (Fig. 12) is a receptacle for a photodiode/LED module. Two of these parts form the ends of the calibrator. Sandwiched between them is part 2 (Fig. 13). This section forms the housing for an ND filter.
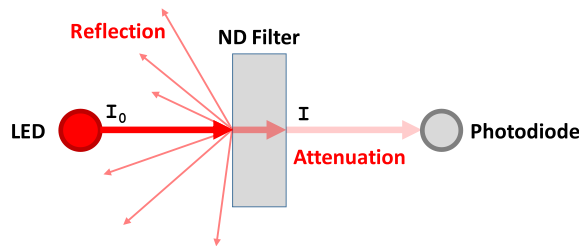
Fig. 10. Attenuation of incident beam I_0 by ND filter to give transmitted beam I.
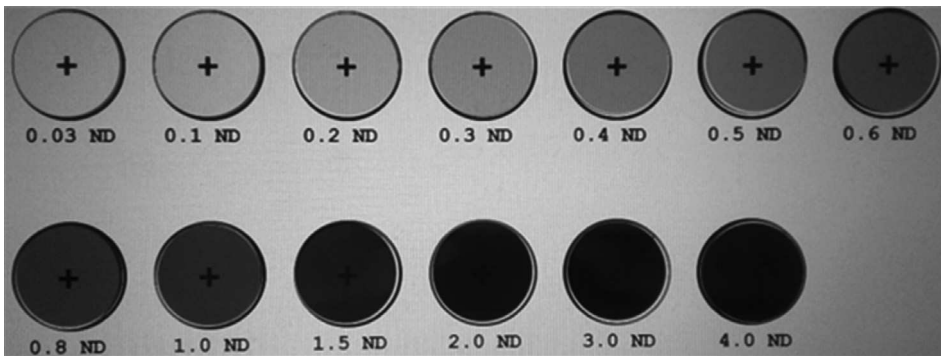
Fig. 11. Neutral density (ND) filters placed on the horizontally oriented monitor of a laptop PC. The 25 mm ND filters attenuate the light from the PC screen.
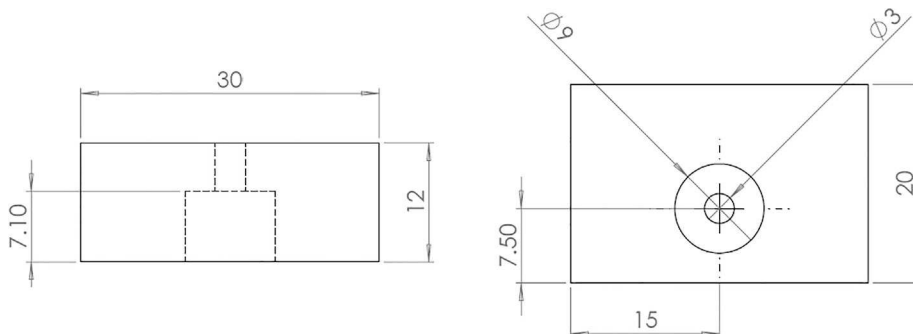
Fig. 12. Photodiode calibrator part 1 – module receptacle.
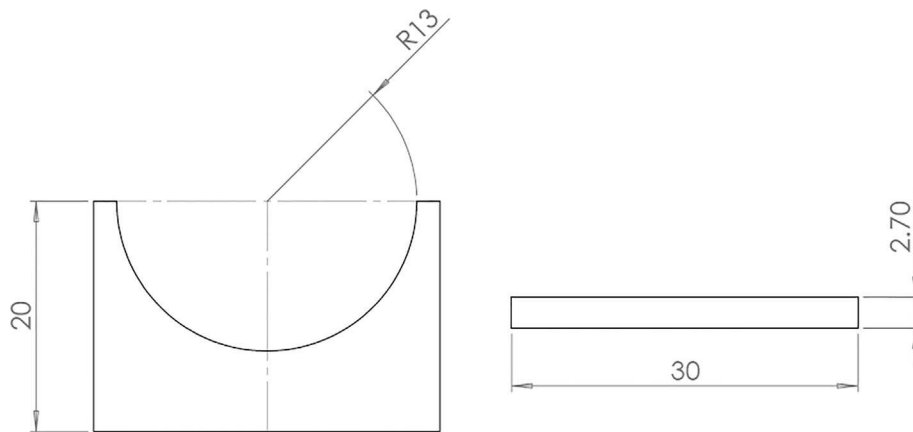
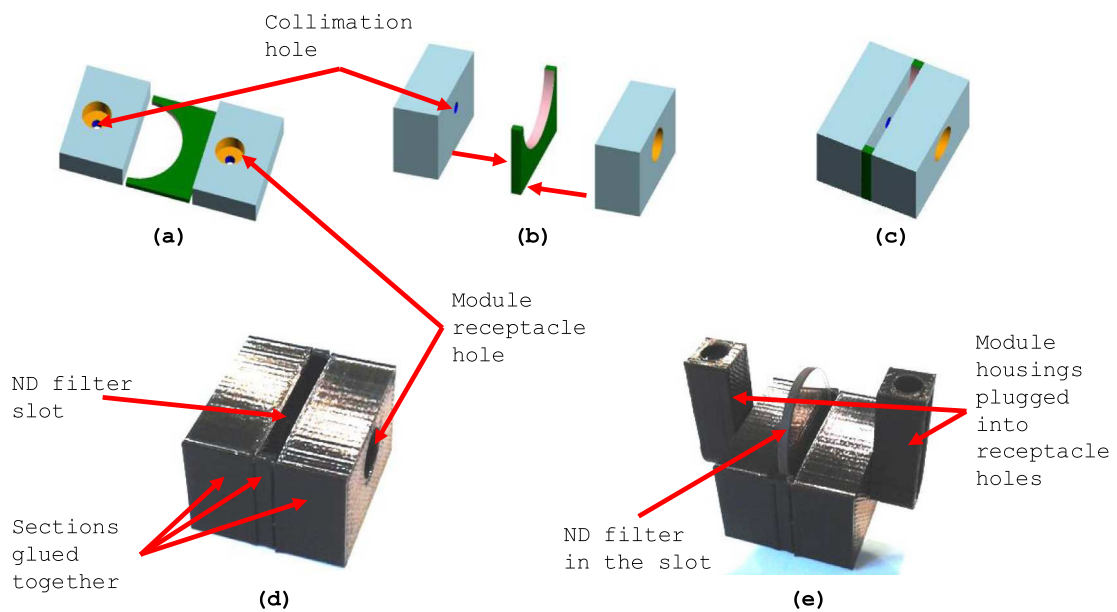**Fig. 13.** Photodiode calibrator part 2 – ND filter housing.

Fig. 14. The optical calibrator. a) CAD model optimised for printing of individual sections on a plastic filament extruding 3D printer. b) CAD model showing the assembly of the separate parts for gluing together. c) CAD model of the assembled unit. d) Photograph of the glued-together optical calibrator unit, showing slot for ND filter insertion and the hole for the LED or sensor module. e) The optical calibrator with two modules plugged in (notionally one LED module and one sensor module), and a 25 mm ND filter located in the slot.

The optical calibrator model was produced using OpenSCAD [8], and printed by a Makerbot 3D printer from PLA plastic filament (Fig. 14). The orientation of part 1 (2 off) and part 2 (1 off) as shown in Fig. 14(a) is flat. This is to optimize the dimensional precision in the 3D printing of the holes and circular sections.

6. Build instructions – electronics & firmware

6.1. Active LED control and current monitoring system

In order to perform precise measurements of optical attenuation using light detectors to measure the transmitted light intensity through a sample, it is first necessary to know precisely the intensity of the LED light source, since the optical transmittance T through a sample is equal to the ratio of the measured light intensity I to the incident light intensity I_0. An instantaneous value for I_0 can be derived from a measurement of the current passing through the LED. The light intensity can then be determined from the luminous intensity vs. forward current graph on the appropriate LED data sheet. This instantaneous current value is required as the current passing through the LED will drift over time due to thermal effects in the control

circuit. A simple circuit based around a ubiquitous LM317 voltage regulator with a digitally controllable feedback section has been designed (Fig. 6) to allow the user to select a desirable LED current, which the circuit will then attempt to establish and maintain over time. Digital control of the active elements in the feedback section is provided by an Arduino UNO microcontroller board running a simple active control algorithm. These active elements are two digital potentiometers (DIGPOTs) and an analogue to digital converter (ADC). The user can communicate with the Arduino UNO via USB to send commands, e.g. the desired current (set-point). The instantaneous LED current measurement can also be polled repeatedly by the user interface, for use in light transmittance calculations.

6.2. Conceptual circuit diagram

The diagram in Fig. 15 illustrates the architecture of the active LED control and current monitoring system, which comprises a control algorithm (Fig. 16) and an electronic circuit (Fig. 17). This circuit is implemented as a "shield" PCB for the Arduino UNO (Fig. 18), where "shield" refers to a secondary "daughter" PCB that can be stacked on top of the "parent" Arduino board and electrically connected by means of SIL headers.

Control of the feedback to the voltage regulator is achieved by the adjustment of two feedback resistors connected in parallel. These feedback resistors are digital potentiometers designated W0 and W1. Each potentiometer wiper can be digitally set to one of 256 discreet values, where the value 0 notionally represents zero resistance, and the value 255 indicates maximum resistance (5 KΩ in this case). This scale provides a resistance resolution of 5000/256 = 19.53 Ω per step. By fixing the value of one potentiometer (W0, or "fine adjust") and then searching for the optimum value of the second potentiometer (W1, or "coarse adjust"), it is possible to achieve the desired set-point current. When the LED current is close to the set point, the control algorithm (Fig. 16) maintains the current level and compensates for drift continuously (for example see Fig. 20). This level of control can be difficult at low currents, i.e. below 1 mA, due to potentiometer resolution limits, or the presence of protective Zener diodes in the LED package. In addition, the forward-voltage to current characteristics of the LED can have a steep gradient in this region (especially so where infrared LEDs are concerned). The minimum load threshold of the voltage regulator is 3.5 mA, and so operating at load currents below this level is outside the specification of the device, adding to the unpredictability of current control in this low current range (Fig. 20), an effect that is further confounded by the increased dominance of voltage measurement noise in this region. However, for most turbidity measurements this effect will not be problematic, as a higher LED intensity would be more desirable for suspended sediment experiments. It will present some small challenges with respect to sensor calibration, however, as low light intensities are useful for the calibration of the high-gain sensors utilised in this application. An obvious solution to the problem of generating a calibration curve at low light
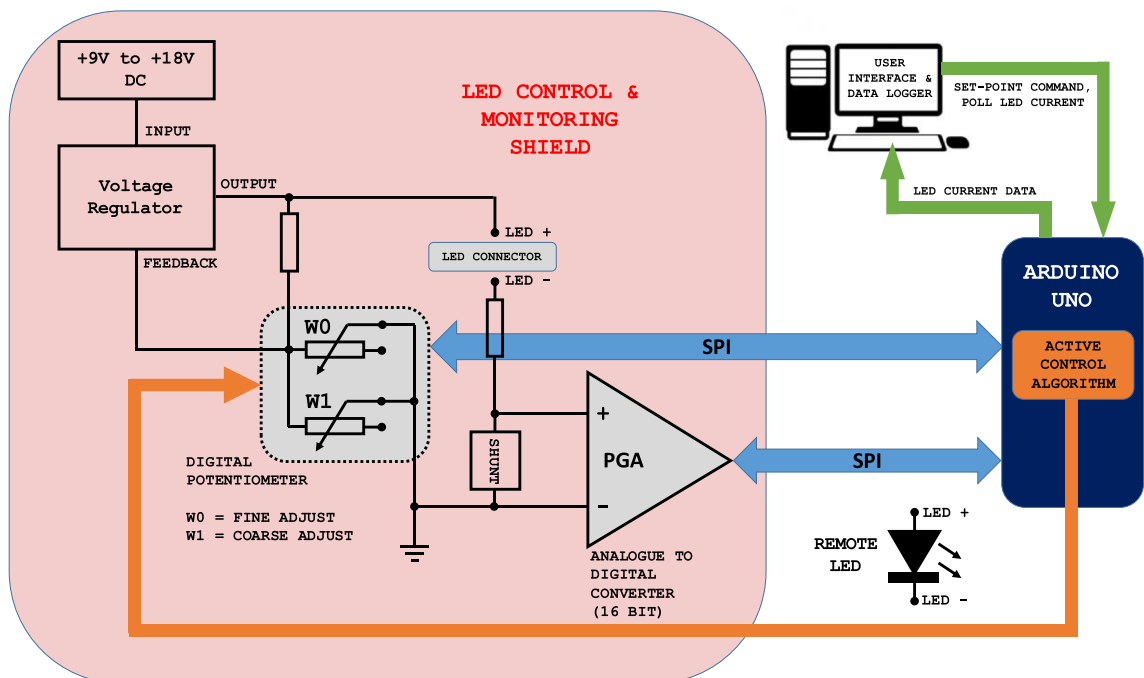

Fig. 15. Conceptual circuit diagram of the LED control system. SPI is the serial peripheral interface for two-way communication between the Arduino UNO and the two chips (the DIGPOT chip and the ADC chip). W0 and W1 are the two potentiometer-wiper positions, controlled digitally via the SPI interface with the Arduino UNO. PGA is the programmable gain amplifier built into the front end of the ADC chip. The box labelled "SHUNT" is the shunt resistor across which the ADC measures a voltage drop. The active control algorithm converts the measured voltage into the LED current measurement.
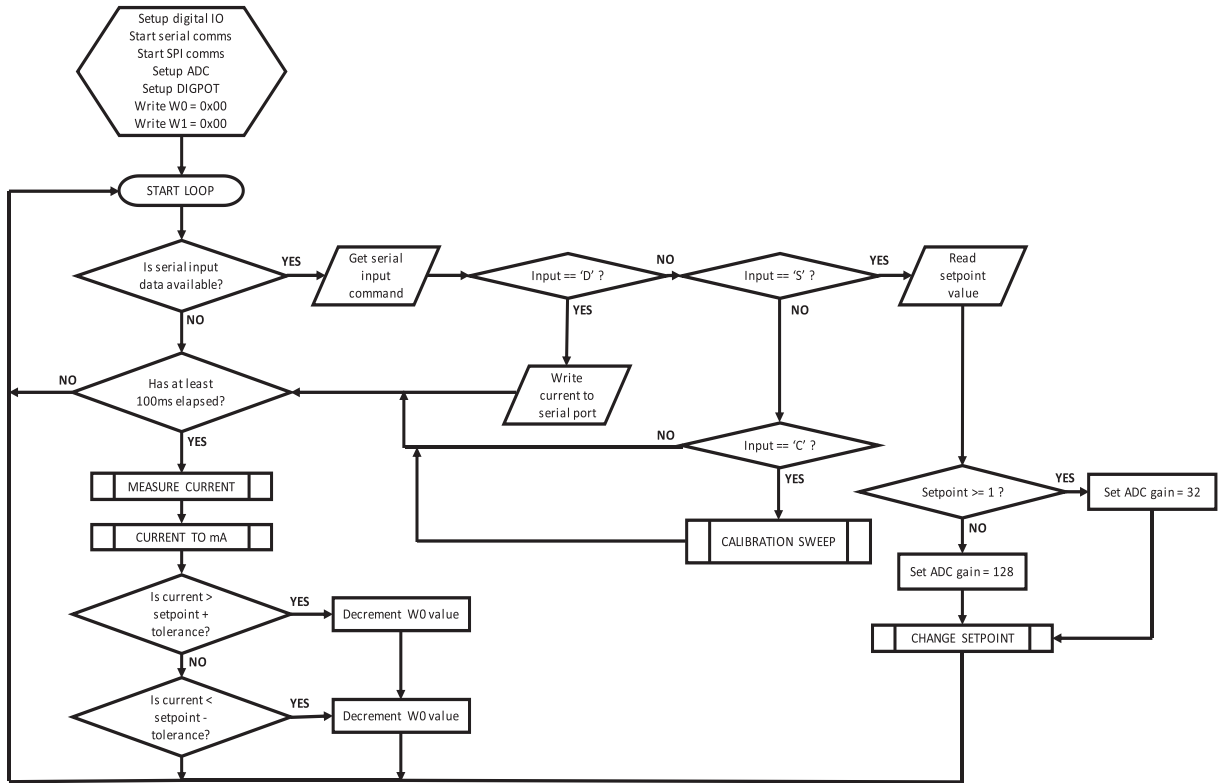
Fig. 16. LED Control algorithm flowchart for Arduino UNO. Shows setup operations and main loop.
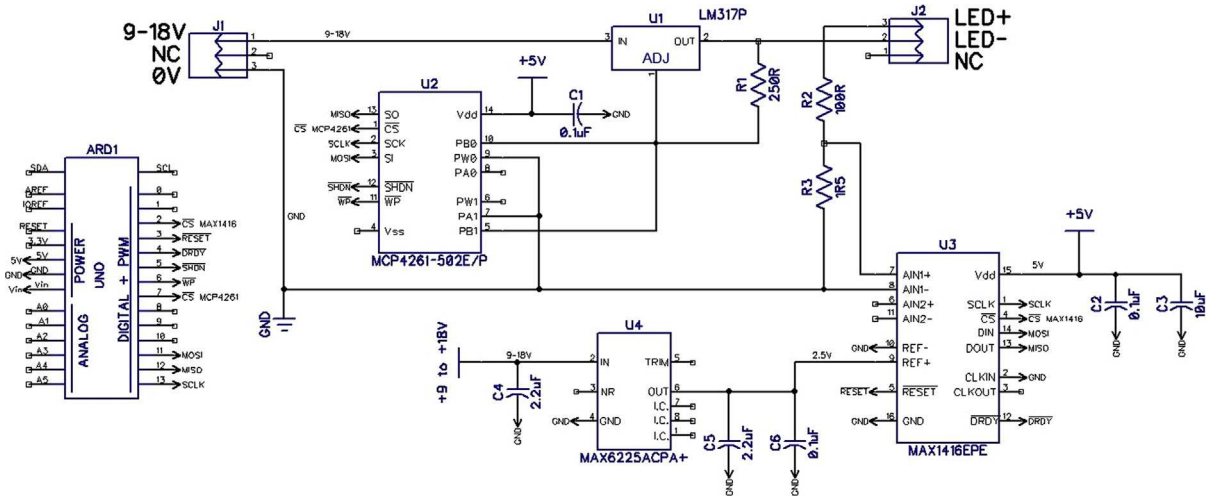

Fig. 17. Circuit schematic of LED control and monitoring shield for Arduino UNO.

levels is to ramp the LED current from a high intensity level to a low intensity level with a high-value ND filter between the LED and the photodiode. We have found that a 3.0 ND filter is ideal for determining the full measurement range of the photodiode amplifier (4.0 ND for λ = 940 nm) whilst keeping the LED at a well-controlled intensity.

6.3. Circuit schematic

The components used for the LED control and monitoring shield were chosen primarily for ease of assembly, i.e. no surface mount devices (SMDs), only dual-in-line (DIP) package integrated circuits (ICs) and through-hole passive components
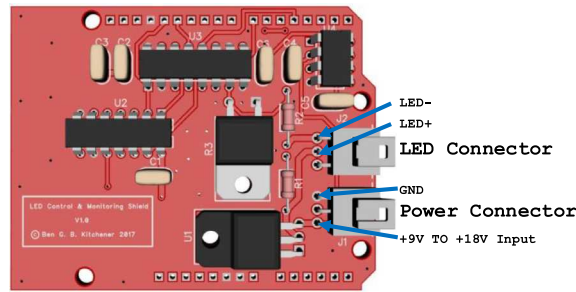
Fig. 18. LED Control & Monitoring Shield PCB for the Arduino UNO.

were chosen. The voltage regulator is an adjustable LM317P [9] in a TO-220FP package, which can be operated from a DC differential input voltage of up to 40 V. The suggested input voltage range for this application is +9 V to +18 V with respect to a common ground, as these voltages can notionally be provided by one or two 9 V batteries connected in series (if portability is required). However, for development and testing purposes a bench power supply was used to provide a nominal 12 V input to the voltage regulator via a Molex connector (J1).

The circuit board has a second Molex connector for plugging a remote LED into the output of the voltage regulator (Fig. 18, J2). This connector puts the LED in series with stabilisation resistor R2, and shunt resistor R3. The shunt resistor provides a ground-referenced measurement to the ADC [10]. This voltage measurement represents the feedback signal to the control algorithm on the Arduino UNO (sent via SPI bus), which can then adjust the values of the two DIGPOTs on board the MCP4261 chip [11] – also via the SPI bus – thus forming direct feedback to the voltage regulator. The MAX6225ACPA+ [12] is a precision 2.5 V voltage reference and is required by the ADC for correct operation.

Fig. 17 shows the net names of all the connections, including to the headers on the Arduino UNO (ARD1). The schematic was created using DipTrace [13], for which a 300-pin limited freeware version is available for non-commercial use.

6.4. Arduino UNO shield PCB

The circuit described by Fig. 17 is realized as a PCB "shield" for the Arduino Uno microcontroller board (Fig. 18). This shield PCB is designed to have the same footprint as the Arduino Uno PCB, and stacks on top of the Arduino by means of SIL headers (2.54 mm pitch), as in Fig. 19.

6.5. Photodiode amplifier design

The photodiode amplifier is a simple transimpedance amplifier that converts the photodiode current into a voltage output. It was designed to be as small as possible to fit in the constrained space available for each of the 18 sensor positions on the outside circumference of the sensor ring. The basic design consists of the SFH213 photodiode [14], an MCP6491 operational amplifier [15], a gain resistor (R1 = 100 MΩ), and two optional capacitors C1 and C2 (Fig. 20). Given the size constraints, a surface-mount design was implemented (Fig. 21), although a through-hole design would be preferable for ease of construction. It is however possible to solder manually the SMD components onto the PCB with a steady hand and a good pair of tweezers.

Solder one end of a short, screened 3-core cable (4.2 – Cable for sensors & LEDS) to the photodiode amplifier PCB. Solder a Molex connector (4.2 – Connector housing for sensors & LEDs) to the other end, and connect the LED module to the LED Control & Monitoring shield via PCB Molex connector (4.2 – J2), as in Fig. 22.
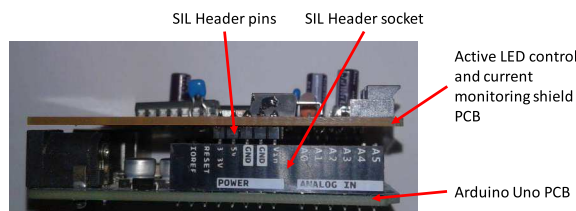

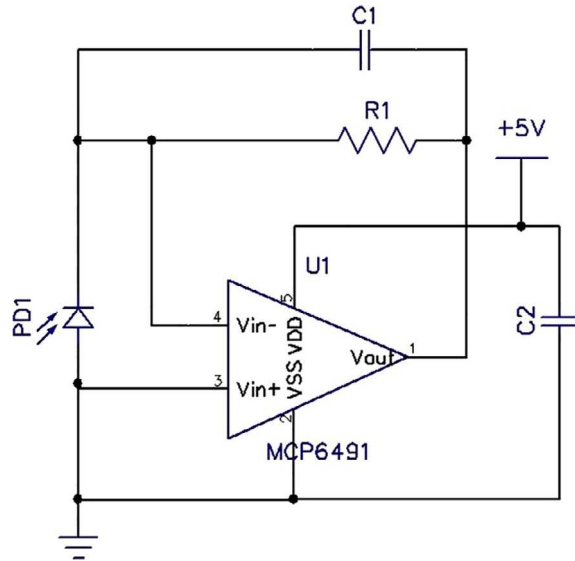**Fig. 19.** Active LED control and current monitoring shield PCB stacked on top of an Arduino Uno.

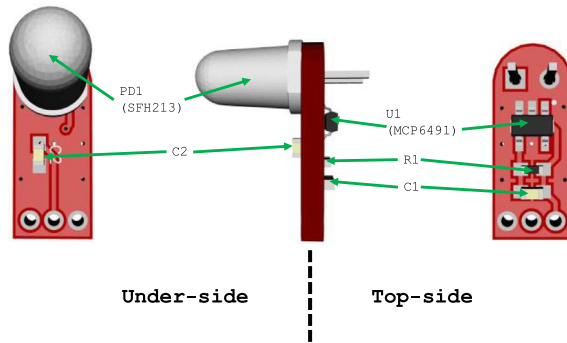**Fig. 20.** Photodiode amplifier schematic.

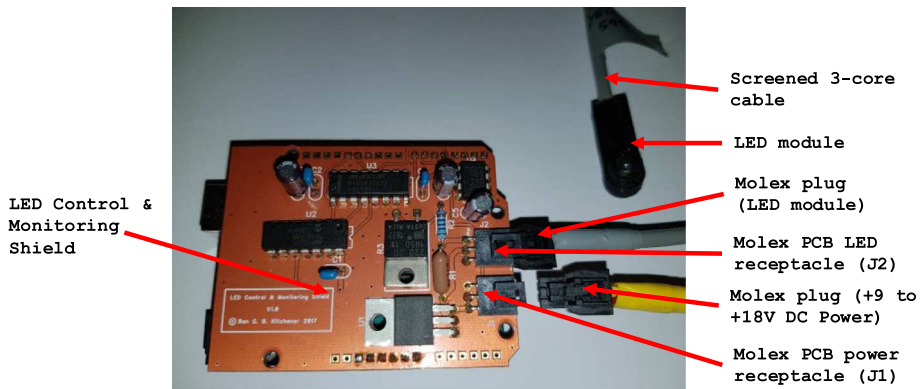**Fig. 21.** Photodiode amplifier PCB.

Fig. 22. LED Control & Monitoring Shield showing LED module connection to J2, and power connection to J1.
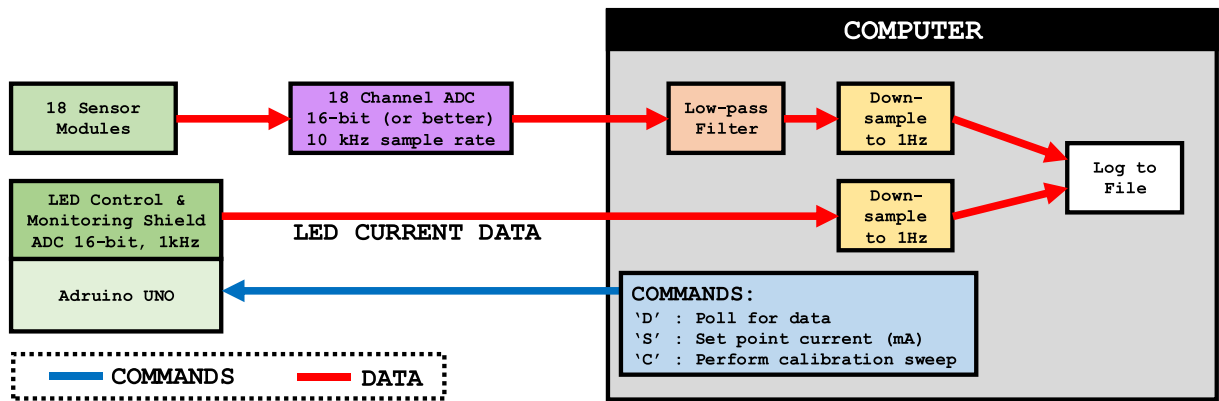
Fig. 23. Suggested generic data-acquisition and logging arrangement.

7. Build instructions – DAQ hardware & software requirements

7.1. Sensor instrumentation and data logging requirements

The photodiode amplifier is particularly sensitive to ambient electric fields due to its high gain configuration. In this design, the amplifier is encased in plastic and potted with epoxy resin. Although this design approach is low-cost, it does not instil any degree of RFI or EMC protection into the circuit. During development, it was observed that the amplifier is particularly sensitive to the presence of ambient 50 Hz interference when a human operator places their hand in close proximity (within a few cm) to the device. The human body is a very good radiator of this background artefact of the domestic power distribution system, hence leaving the device undisturbed during operation is recommended. A countermeasure to this undesirable effect is to sample the photodiode amplifier signal at a rate of 10 k samples per second (SPS), allowing for the application of a digital low-pass filter to remove 50 Hz power line interference and other transients (3rd-order Butterworth infinite impulse response (IIR) filter with 1 Hz cut-off frequency). We applied this approach to all 18 data channels, but only recorded the filtered data to disk at a rate of one sample per second. Also recorded at a rate of 1 SPS was the instantaneous LED current as measured by the active LED control and current monitoring system (Fig. 23). This measurement allows each of the 18 measured data points to be compensated for LED intensity, as inferred from the recorded LED current value.

The resolution at which the sensor voltage is measured is recommended to be less than 1 mV if possible. In some situations, the side-scattered signal from suspended sediment will lead to some very small responses in the detectors situated around the 90° position, so to see any structure in the recorded time-domain signal the best voltage resolution possible is desirable. We used a DAQ system with a voltage input range of ±10 V, and an ADC resolution of 16 bits. This system gave us a voltage measurement resolution of 0.305 mV. However, if the voltage input range of the DAQ were to be limited to 0–5 V, then the exact same voltage resolution could be achieved with only 14 bits of ADC resolution.

7.2. User DAQ

This article does not describe a data acquisition and logging system. The operators must therefore select their own system. The data presented in this article were obtained using National Instruments (NI) DAQ equipment, and was programmed using NI LabVIEW graphical programming environment [16]. The production of a low-cost, open-source DAQ system is the subject of future work.

7.3. Example LabVIEW GUI

The DAQ system that we implemented using NI equipment has a LabVIEW GUI (Fig. 24) that controls the operation of the LED Control & Monitoring system and reads the instantaneous LED current. It also logs 18 channels of data from the connected NI DAQ hardware, which was in this case 16 channels from an NI USB-6211 [17] plus 2 channels from an NI myDAQ [18].

8. Operation instructions – experimental methodology & data logging

8.1. Hazards associated with high-brightness LEDs

Warning: All LEDs that emit focused IR or UV light can be dangerous to the eyes, and UV LEDs can potentially damage the skin. Even the visible light LEDs when operated at nominal currents (e.g. 30 mA) can cause damage to the eye due to high output intensities (sometimes tens of thousands of millicandela). It is therefore recommended that anyone operating high-
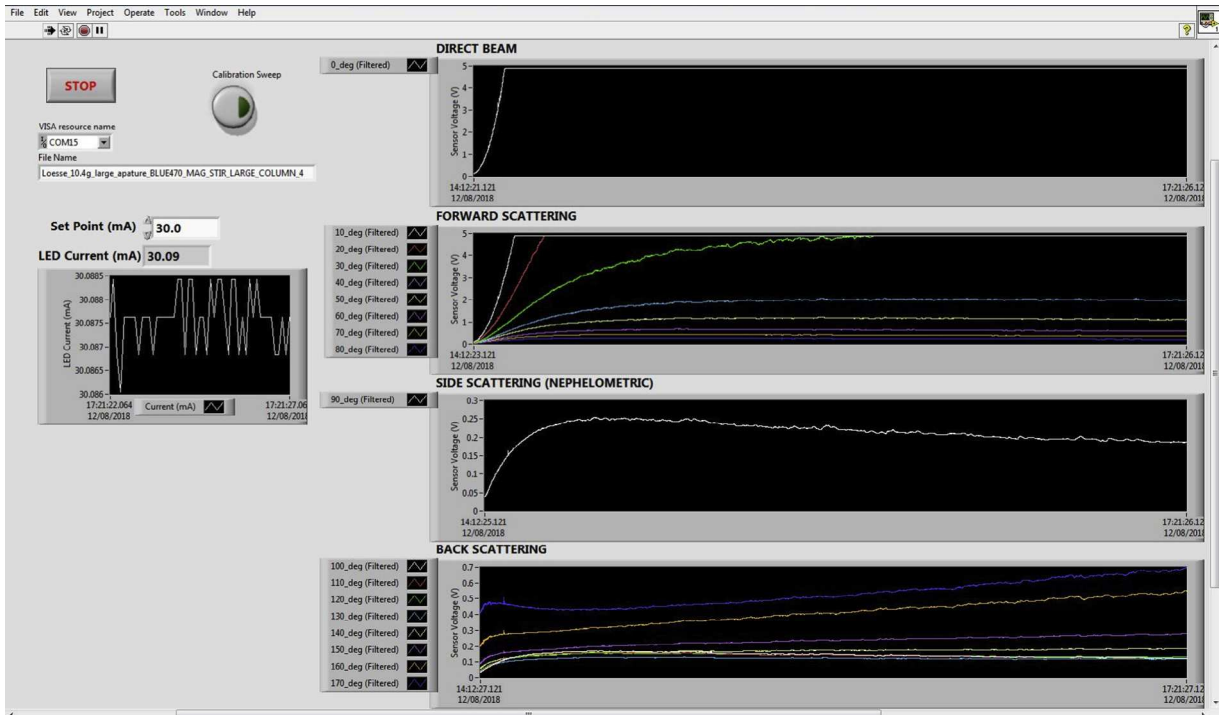
Fig. 24. Example LabVIEW GUI for TARDIIS.

intensity visible, IR or UV LEDs should never look directly into the lens of the LED. This is of paramount importance where IR LEDs are concerned, as they will appear to be un-powered even when operating at nominal intensity, since IR light is not visible to the human eye. As such the human eye will have no pupil reflex with which to attenuate the incoming light, and permanent damage can be caused to the retina – including blindness. It is good practice to treat high-brightness LEDs with the same caution as one would a LASER light source.

8.2. Sensor calibration

The following list is a complete calibration example. The operations are to be performed in this order:

1. Connect DAQ system together, wire up all sensors etc., apply power and test all DAQ channels and functionality.
2. Choose a light source. In this example an IR LED (λ = 940 nm) has been selected [19]. Plug it into J2 on the Control & Monitoring shield.
3. Determine the relationship between LED current and output light intensity in mW/sr by extracting information from the LED data sheet. In Fig. 25 the radiant intensity is stated in milli Watts per steradian (mW/sr). If the radiant intensity is stated in photometric units of millicandela (mcd), then the mcd value must be multiplied by the conversion factor V (λ) to obtain the radiometric value in mW/sr (Eq. (3)). Wavelength λ is stated in nm [20,21]:

$$V(\lambda) = 1.019e^{-285.4(0.001(\lambda-559))^2} \tag{3}$$

For example, a blue LED of wavelength 470 nm, $V(\lambda)$ = 0.106264. This conversion is necessary since the candela is weighted according to the wavelength-dependent sensitivity of the human eye to light. Since photodiodes do not have this non-linear human-eye response, photometric units such as candelas (or mcd) must not be used to report the measured light intensities.

$$I_{mW/sr} = \frac{I_{mcd}}{V(\lambda)} \tag{4}$$

Using data extracted from the graph in Fig. 25, the relationship between the applied current and the 940 nm LED light output can be stated: I_{OUT} (mW/sr) = 1.978 $\times$ I_{IN} (mA), as shown in Fig. 26. The constant multiplier 1.978 shall be referred to as m_{LED}. So the expression for the input current to output light intensity is:
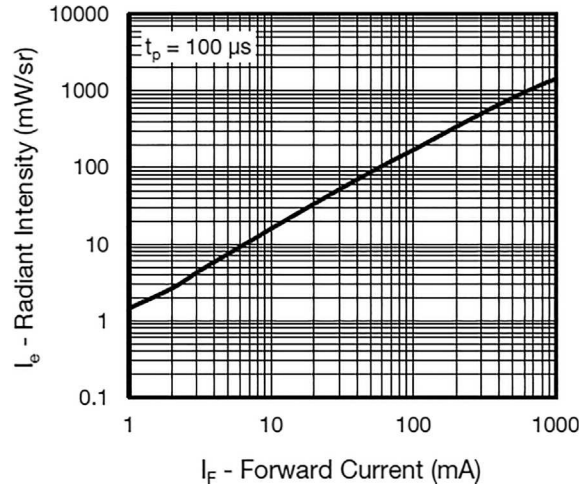
$$I_{OUT} = m_{LED}I_{IN} \tag{5}$$

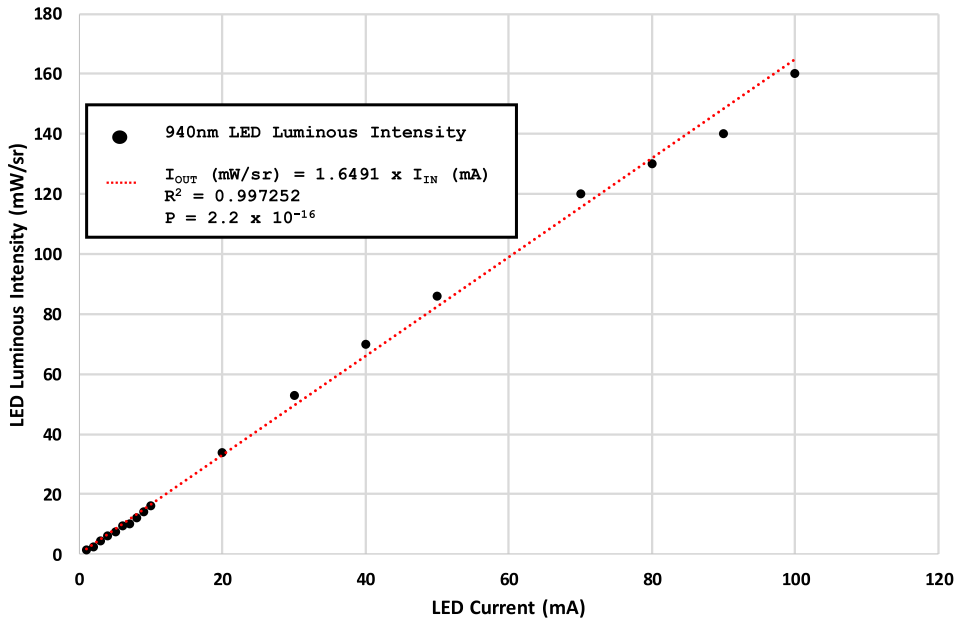**Fig. 25.** Radiant intensity vs. forward current. Extracted from Vishay TSAL6100 data sheet [19].

Fig. 26. LED current input vs. light output intensity as derived from Vishay TSAL6100 data sheet [19]. The data points were extracted from the data sheet "by eye". Even so, there is a good fit to a linear regression (R^2 = 0.9947, p = 2.2 × 10^{-16}) making the data suitable for calibration purposes.

4. Obtain a value for the transmittance through the chosen ND filter by examining the calibration graph supplied by the manufacturer and correcting for wavelength to arrive at transmission T_λ. The nominal transmittance of a 4.0 ND filter is 0.0001 (0.01%). Correcting for wavelength response at 940 nm from the manufacturer's ND calibration data, this value is modified to become T_{940nm} = 0.00038 (0.038%). Applying Eq. (2), the 4.0 ND filter value becomes 3.42 ND_{940nm}. Extending Eq. (5) to include the attenuation by the ND filter gives Eq. (6) below:

$$I_{OUT} = m_{LED}I_{IN}T_\lambda \tag{6}$$

5. Determine the response of each individual sensor module to the light source using the optical calibrator, and plot the relationship between sensor voltage and incident light level (mW/sr). The Arduino software has a "calibration sweep" function that performs a stepwise drop in LED current from the present set point. The current dwells at each step for one second for stabilization, thus allowing a calibration graph to be plotted. The gradient of the linear regression fit of sensor voltage S_V to the measured light intensity I_θ (θ is the scattering angle) yields the sensor calibration coefficient S_α, where α is the sensor number. The measurements shown in Fig. 27 were made with a 4.0 ND (3.42 ND_{940nm}) filter in place to attenuate the beam (otherwise the sensor output would saturate).

We now have a general calibration equation that can be applied to experimental data to give I_θ at a given scattering angle θ in mW/sr:

$$I_\theta = S_\alpha S_V \tag{7}$$

The calibration sweep was performed by starting at an initial LED current of 30 mA and ramping the current down from there. Applying general calibration Eq. (7) we now obtain a specific calibration equation for sensor #9 at the 90° position on the sensor ring:

$$I_{90} = S_9 S_V = 0.005959 S_V \tag{8}$$

The I_{90} equation (above) will be used in the experimental measurement section.

6. With all the sensor modules in position around the sensor ring, add clean water to the sample cell (in this case tap water). Remove all ambient light (i.e. total darkness) and measure the response of all the sensor modules to the LED light source located at the 180° position. Any response measured at sensor locations from 10° to 170° are due to internal reflections within the instrument (Fig. 28).

The response of the sensor at the 0° position is due to the direct beam, and is likely to cause the sensor to saturate. This effect could also be apparent at high beam intensities at the 10° and 20° positions (and other forward-angle positions), due to the divergence of the incident beam. The LED intensity can be stepped from high to low in order to generate a device geometry baseline (DGB_λ) dataset for each sensor. The "calibration sweep" function in the Arduino firmware can be used again to achieve this functionality. Fig. 29 shows data for high (29.02 mA) and low (5.38 mA) LED intensities. Scattering angles θ_0 and θ_{10} have saturated detector responses at both intensities. The effect of the beam divergence on the forward-scattering sensors can be seen to drop off as θ approaches 90°. The effects of internal reflections can be seen to increase in the back-scattering sensors as θ approaches 170°. The sensors are numbered from 0 to 17, and are placed at corresponding $\theta \times 10°$ angular positions around the sensor ring. For example, sensor #9 at 90° (Fig. 27) is located at the θ_{90} position.

8.3. Performing a sediment-settling experiment

1. Choose a light source. In this example a 940 nm LED (infrared) was selected, at a nominal operating current of 30 mA. The diagrams (Figs. 30 and 31) illustrate the experiment using blue light for clarity, since infrared light is not visible to the human eye.

2. Perform an experiment on a suspended sediment sample. The experiment design is at the discretion of the user, for example the choice of initial agitation method (e.g. stirring, dropping sediment into the water column, shaking the sample, measurement frequency, duration of experiment). The sample was stirred with a magnetic stirrer until a consistent degree of suspension was achieved. The settling experiment begins when the stirrer is switched off.

Δ   Sensor #9 response

I (mW/sr) = 0.005959 x S_V (Volts) x 0.00038
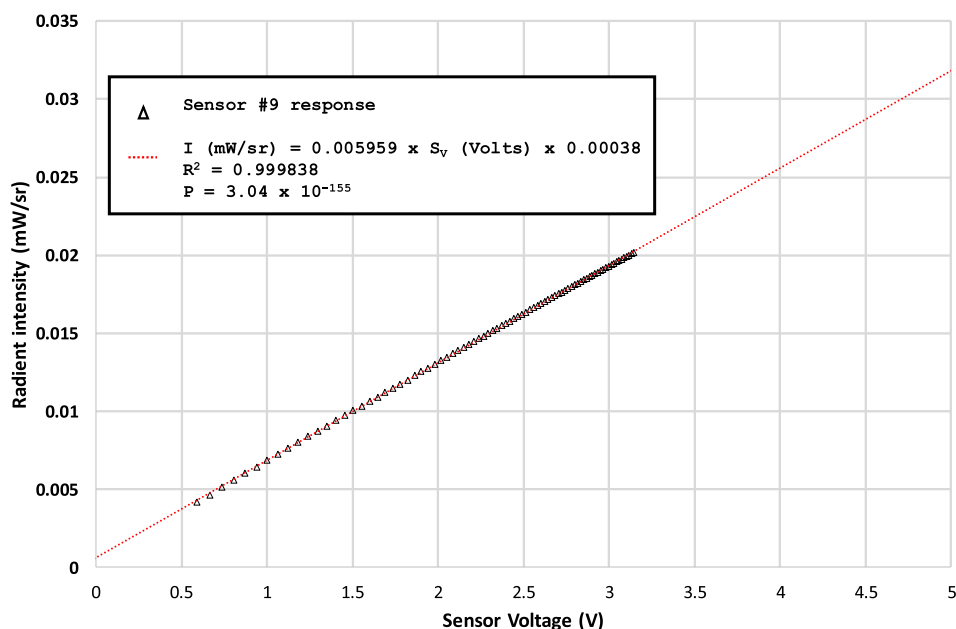R^2 = 0.999838
P = 3.04 x 10^{-155}

Fig. 27. Response of sensor #9 to 940 nm light. Data generated using 'calibration sweep' function with optical calibrator and 4.0 ND filter, starting at 30 mA LED current.
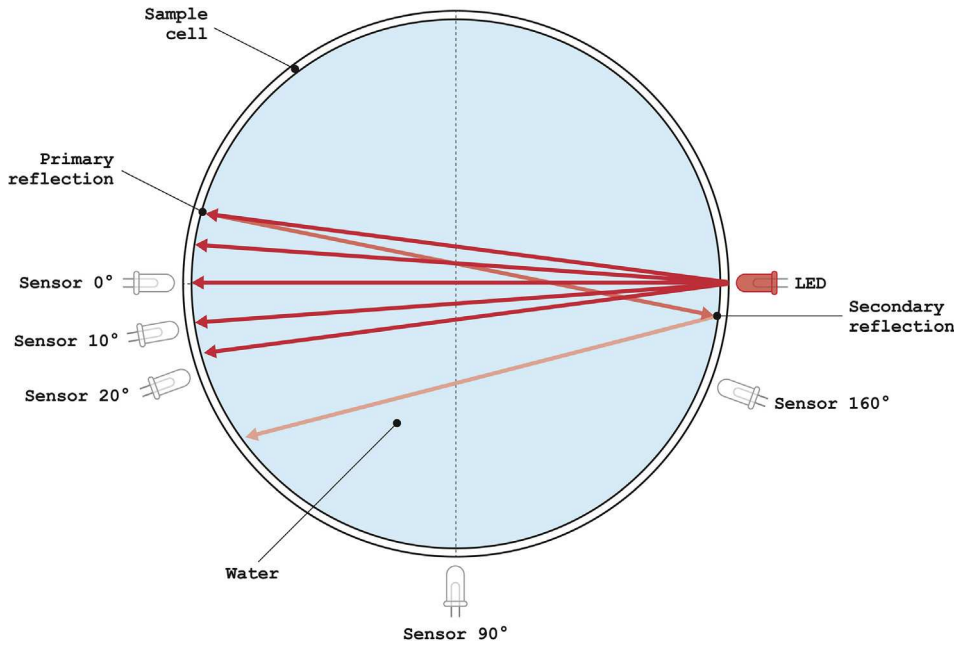
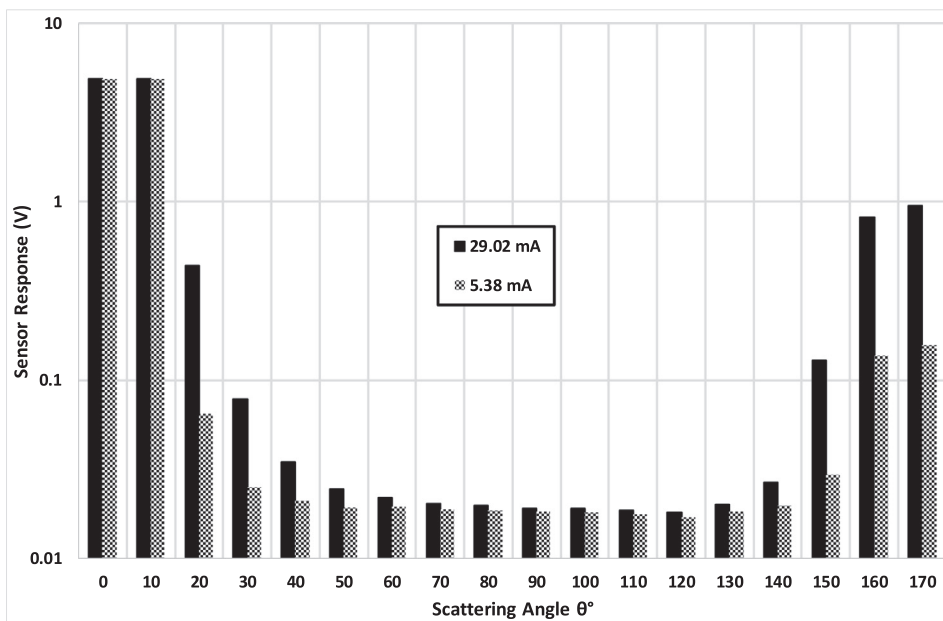**Fig. 28.** Reflections from the internal surfaces of the sample cell.

Fig. 29. Water-only calibration of the TARDIIS sample cell, referred to as the Device Geometry Baseline (DGB_{940nm}) data set. Two LED currents are shown (29.02 mA and 5.38 mA), representing high and low LED intensities. In this example the 0° and 10° sensor responses have saturated.

8.4. Preparing the data

It is important to know what events have been recorded during the experiment, and to know when the settling process begins. In our experiments, the entire process including the agitation phase is recorded. Thus, it is necessary to remove manually the beginning section of each data set in order to remove the effects of the stirring process. Also during this start-up phase, the LED is ramping up to its set-point current, and so this initial data is not meaningful. Only when the LED is at a stable current and the stirring has stopped can the data considered to be at the *time = 0* position, t_0 (Fig. 32).
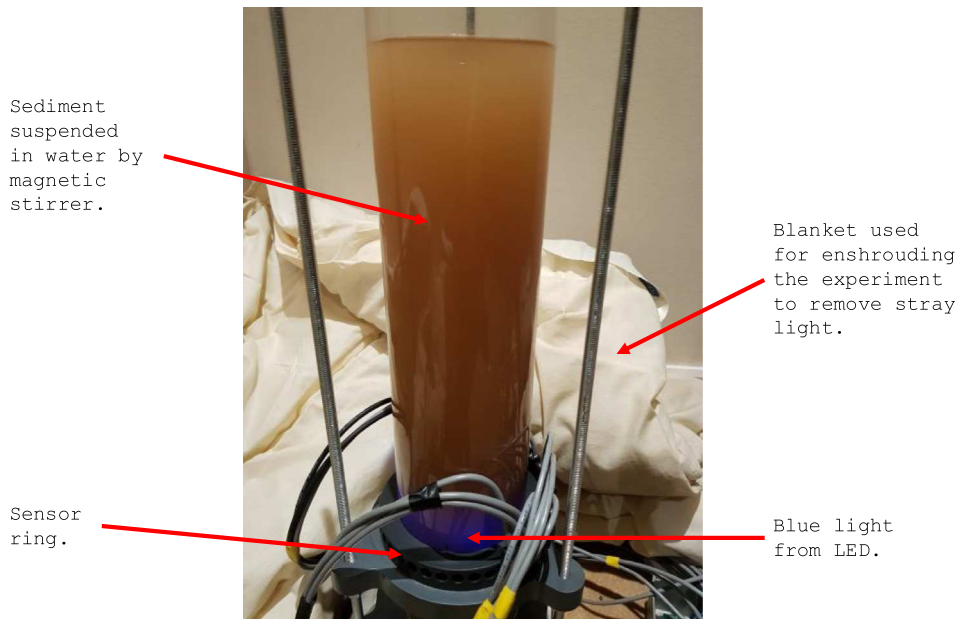
Fig. 30. Photograph of a sediment settling experiment.
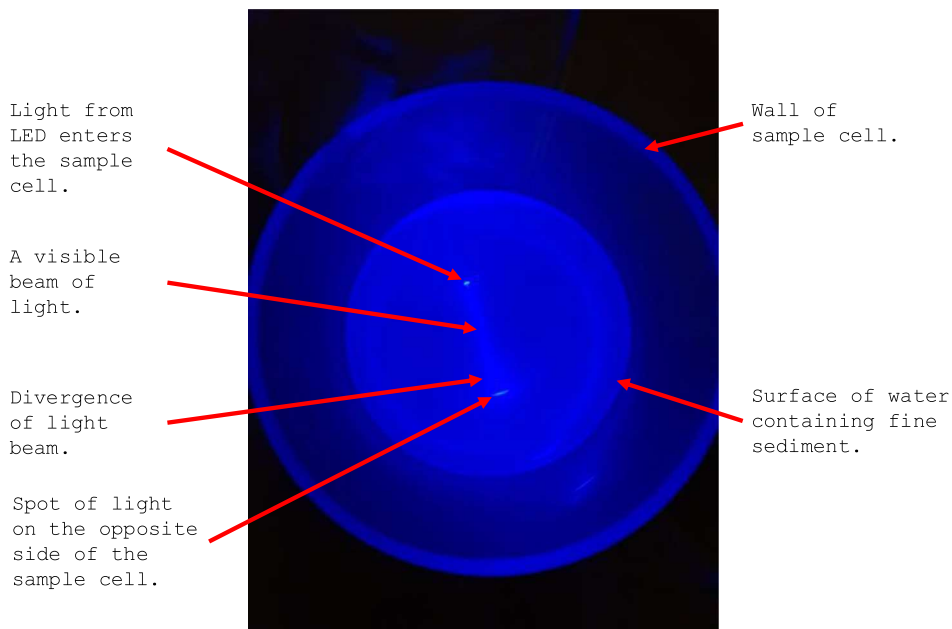

Fig. 31. Top view of the sample cell. Side-scattering from the beam of blue light is evident, as are various reflections from the inner surface of the sample cell. (For interpretation of the references to colour in this figure legend, the reader is referred to the web version of this article.)

9. Validation, characterization and modelling

TARDIIS allows the researcher to obtain a rich and diverse set of data about sediment as it settles in a column of water. These data do not however show directly the concentration of sediment at a particular height in the water column. The only way to measure *exactly* the characteristics of the sediment at different positions in the settling column and at different times during the settling process, is by physically sampling the column. Then, by the use of traditional sediment analysis methods, it is possible to determine the concentration, the PSD, the grain shapes, the degree of flocculation (DOF) and so on. The researcher must accept that there is not a well-defined link between sediment properties and turbidity in general. With this
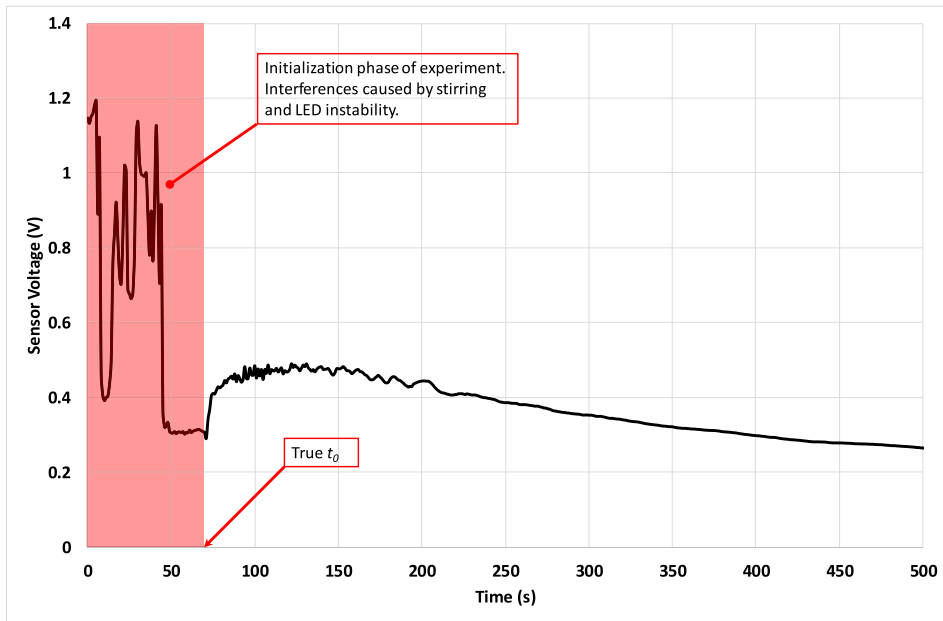
Fig. 32. Graph showing the initialization phase of a sediment-settling experiment. $\lambda = 940$ nm, $\theta = 30°$. The sediment used is loess, at a density of 0.5168 gl^{-1}. The hight of the water column is 426 mm and the sensor ring height is 102 mm.

acceptance, the researcher may then challenge existing approaches to turbidity measurements, and use TARDIIS to establish new models that are based on the physics of light scattering and absorption.

9.1. Assessment of the active LED control and current monitoring system

The instantaneous current was measured throughout the settling experiment, thus allowing for the correction of the calculated I_0 value. The current is plotted against time (Fig. 33) and shows that the drift in I_0 is very small – i.e. not greater than 72 μA – over the 10.67 h duration of the example experiment. There is a small amount of noise present in the signal; however, the overall degree of drift shows that the Arduino control system is performing very well, as the desired current is 30 mA in this case. There is an overall offset error of approximately 40 μA.
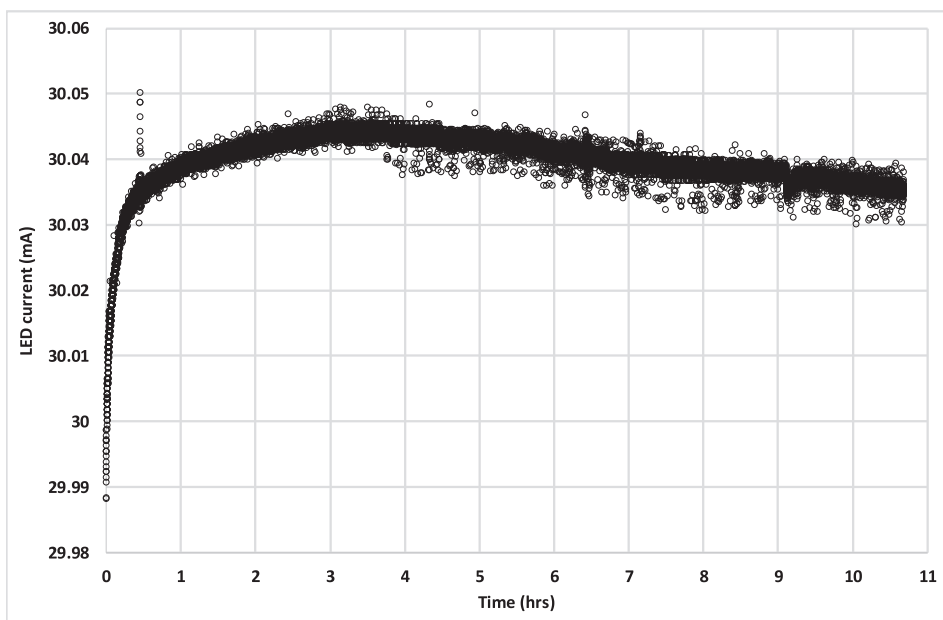

Fig. 33. LED current drift.

9.2. Linearity of device geometry baseline measurements

It has been shown that the response of a specific sensor (#9) to incident light is linear (Fig. 27) when calibrated using an ND filter. We must now check that the response function is linear when TARDIIS is operational. Using data that was collected to produce Fig. 29, we can now show that the same linearity is present under device geometry baseline (DGB) conditions, with only water present in the sample cell. The responses of sensors #6, #9 and #12 are shown as I_{60}, I_{90} and I_{120} respectively in Fig. 34, which confirms that the linearity is present. This DGB linearity must be tested for all sensors at all wavelengths of light that are to be used during settling experiments.
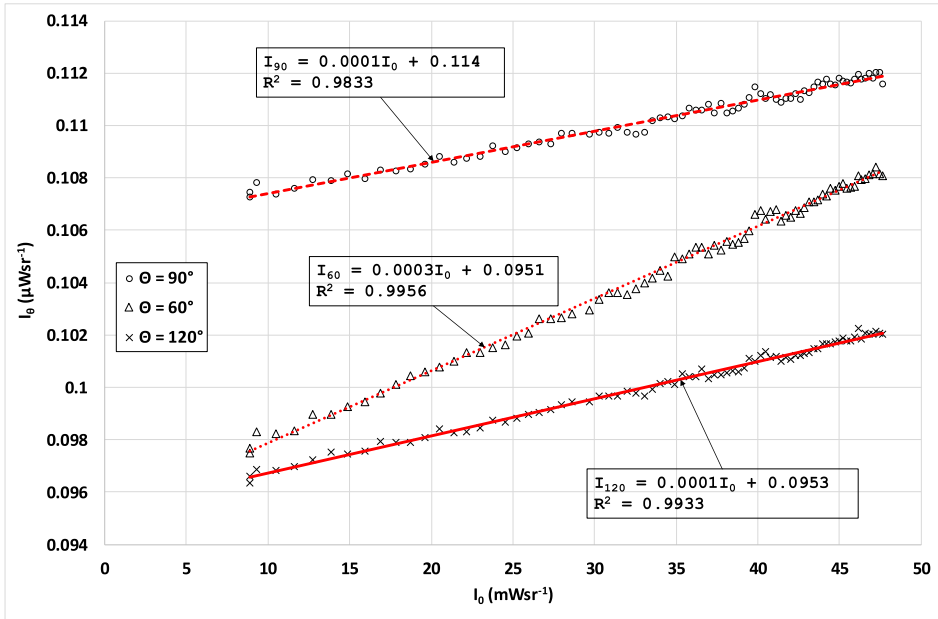

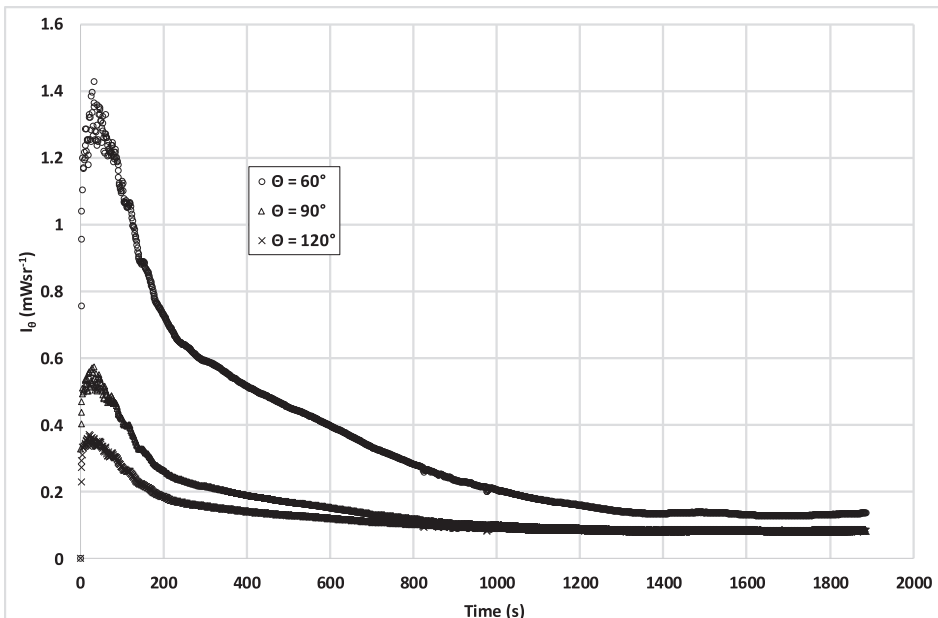**Fig. 34.** Linearity of DGB measurements I_{60}, I_{90} and I_{120}.

Fig. 35. A sediment settling experiment using a loess concentration of 0.5168 gL^{-1}. $\lambda = 940$ nm.

9.3. Example of sediment-settling data

The data in Fig. 35 show the measured light intensity at three of the 18 available scattering angles during a sediment settling experiment. The initial peak that occurs at around 30 s into the experiment is due to turbulence in the water column after the magnetic stirrer is switched off. By analysing data gathered in this way at multiple scattering angles and wavelengths of light, the researcher may then:

- Develop models of light scattering by particles in suspension, and gain new insights into the effects of grain shape and PSD.
- Explore the impact that water colour has on turbidity measurement.
- Investigate the conditions under which the particle settling velocities deviate from Stokes Law.
- Enquire as to the suitability of the recognized turbidity standards.
- Apply new knowledge to future field measurements.

The "optical sedigraphs" shown in Fig. 35 look as if they may be giving an indication of Stokes-like settling behaviour. In order to explore this possibility, the researcher must design their experiments carefully, and then develop suitable numerical models to make predictions based on empirical data obtained using TARDIIS. This detailed analysis and model development is however beyond the scope of this article.

Declaration of interest

None declared.

Acknowledgements

Appendix A. Supplementary data

Supplementary data to this article can be found online at https://doi.org/10.1016/j.ohx.2019.e00052.

References

[1] B.G.B. Kitchener, J. Wainwright, A.J. Parsons, A review of the principles of turbidity measurement, Prog. Phys. Geogr. 41 (2017) 620–642, https://doi.org/10.1177/0309133317726540.

[2] D.M. Lawler, R.M. Brown, A simple and inexpensive turbidity meter for the estimation of suspended sediment concentrations, Hydrol. Process. 6 (1992) 159–168.

[3] T.P. Lambrou, C.C. Anastasiou, C.G. Panayiotou, A nephelometric turbidity system for monitoring residential drinking water quality, in: Sens. Appl. Exp. Logist. First Int. Conf. SENSAPPEAL 2009, Athens, Greece, Sept. 25, 2009, Revis. Sel. Pap., Springer Berlin Heidelberg, 2009, pp. 43–55, doi: 10.1007/978-3-642-11870-8_4.

[4] L. Bilro, S.A. Prats, J.L. Pinto, J.J. Keizer, R.N. Nogueira, Design and performance assessment of a plastic optical fibre-based sensor for measuring water turbidity, Meas. Sci. Technol. 21 (2010), https://doi.org/10.1088/0957-0233/21/10/107001 107001.

[5] C.D. Kelley, A. Krolick, L. Brunner, A. Burklund, D. Kahn, W.P. Ball, M. Weber-Shirk, An affordable open-source turbidimeter, Sensors (Basel) 14 (2014) 7142–7155, https://doi.org/10.3390/s140407142.

[6] J.F. Orwin, C.C. Smart, An inexpensive turbidimeter for monitoring suspended sediment, Geomorphology. 68 (2005) 3–15, https://doi.org/10.1016/j.geomorph.2004.04.007.

[7] Ragworm PCB Fabrication, (2018). https://ragworm.eu/ (accessed August 12, 2018).

[8] M. Kintel, C. Wolf, OpenSCAD, The Programmers Solid 3D CAD Modeller, (2018). http://www.openscad.org/.

[9] ST Microelectronics, LM317, n.d. https://www.st.com/resource/en/datasheet/lm217.pdf (accessed August 28, 2018).

[10] Maxim, MAX1415/MAX1416, 16-Bit, Low-Power, 2-Channel, Sigma-Delta ADCs, (2015) 35. https://datasheets.maximintegrated.com/en/ds/MAX1415-MAX1416.pdf.

[11] Microchip, MCP414X/416X/424X/426X, 7/8-Bit Single/Dual SPI Digital POT with Non-Volatile Memory, (2008) 88. http://ww1.microchip.com/downloads/en/DeviceDoc/22059b.pdf.

[12] Maxim, MAX6225/MAX6241/MAX6250, Low-Noise, Precision, +2.5V/+4.096V/+5V Voltage References, (2014) 11. https://datasheets.maximintegrated.com/en/ds/MAX6225-MAX6250.pdf.

[13] Novarm, DipTrace, schematic and PCB design software, (2018). https://diptrace.com/download/download-diptrace/.

[14] Osram, SFH213, Silicon PIN Photodiode, (2018) 13. https://dammedia.osram.info/media/resource/hires/osram-dam-5488355/SFH 213_EN.pdf.

[15] Microchip, MCP6491/2/4, 7.5 MHz, Low-Input Bias Current Op Amps, (2012) 50. https://www.microchip.com/wwwproducts/en/MCP6491.

[16] National Instruments: Test, Measurement, and Embedded Systems – National Instruments, (2018). http://www.ni.com/en-gb.html (accessed July 21, 2018).

[17] National Instruments, USB-6211 – National Instruments, (2018). http://www.ni.com/en-gb/support/model/usb-6211.html (accessed August 12, 2018).

[18] National Instruments, myDAQ Student Data Acquisition Device – National Instruments, (2018). https://www.ni.com/en-gb/shop/select/mydaq-student-data-acquisition-device (accessed August 12, 2018).

[19] Vishay, TSAL6100, High Power Infrared Emitting Diode, 940 nm, GaAlAs, MQW, Vishay Intertechnology. (2017). https://www.vishay.com/ir-emitting-diodes/list/product-81009/ (accessed July 21, 2018).
[20] THORLABS, Radiometric vs. Photometric Units, 2018. https://www.thorlabs.de/catalogPages/506.pdf.
[21] L.T. Sharpe, A. Stockman, W. Jagla, H. Jägle, A luminous efficiency function, $V*(\lambda)$, for daylight adaptation, J. Vis. 5 (2005) 3, https://doi.org/10.1167/5.11.3.